nature communications

Article

https://doi.org/10.1038/s41467-024-54384-x

A potent broad-spectrum neutralizing antibody targeting a conserved region of the prefusion RSV F protein

Received: 20 April 2024

Accepted: 7 November 2024

Published online: 21 November 2024

Check for updates

Yongpeng Sun[1,2,4], Liqin Liu[1,2,4], Hongsheng Qiang[1,2,4], Hui Sun[1,2,4], Yichao Jiang[1,2,4], Luo Ren[3,4], Zemin Jiang[1,2,4], Siyu Lei[1,2], Li Chen[1,2], Yizhen Wang[1,2], Xue Lin[1,2], Guosong Wang[1,2], Yang Huang[1,2], Yuhao Fu[1,2], Yujin Shi[1,2], Xiuting Chen[1,2], Hai Yu[1,2], Shaowei Li[1,2], Wenxin Luo[1,2], Enmei Liu[3] ✉, Qingbing Zheng[1,2] ✉, Zizheng Zheng[1,2] ✉ & Ningshao Xia[1,2] ✉

Respiratory syncytial virus (RSV) poses a significant public health challenge, especially among children. Although palivizumab and nirsevimab, neutralizing antibodies (nAbs) targeting the RSV F protein, have been used for prophylaxis, their limitations underscore the need for more effective alternatives. Herein, we present a potent and broad nAb, named 5B11, which exhibits nanogram level of unbiased neutralizing activities against both RSV-A and -B subgroups. Notably, 5B11 shows a ~20-fold increase in neutralizing efficacy compared to 1129 (the murine precursor of palivizumab) and approximately a 3-fold increase in neutralizing efficacy against B18537 in comparison to nirsevimab. Cryo-electron microscopy analysis reveals 5B11's mechanism of action by targeting a highly conserved epitope within site V, offering a promising strategy with potentially lower risk of escape mutants. Antiviral testing in a female cotton rat model demonstrated that low-dose (1.5 mg/kg) administration of 5B11 achieved comparable prophylactic efficacy to that achieved by high-dose (15 mg/kg) of 1129. Furthermore, the humanized 5B11 showed a superior in vivo antiviral activity against B18537 infection compared to nirsevimab and palivizumab. Therefore, 5B11 is a promising RSV prophylactic candidate applicable to broad prevention of RSV infection.

Respiratory syncytial virus (RSV) is the leading cause of hospitalization in children under five 5 years old with acute respiratory tract infections (ARIs)[1]. RSV infection contributes to a tremendous disease burden in older adults[2] and children aged ≤2 years, particularly infants under 6 months of age[3], posing a 14-fold higher risk of severe pneumonia in children[4]. In 2019, RSV was responsible for approximately 33.0 million ARIs episodes, 3.6 million hospital admissions, and 101,400 deaths globally among children under five years of age[5]. The US Food and Drug Administration (FDA) recently approved GSK's Arexvy and Pfizer's ABRYSVO vaccines, both based on the prefusion F (pre-F) proteins, to prevent lower respiratory tract disease in individuals aged 60 years and above[6]. Additionally, Moderna has announced encouraging

[1]State Key Laboratory of Vaccines for Infectious Diseases, Xiang An Biomedicine Laboratory, School of Public Health, Xiamen University, Xiamen, P. R. China. [2]National Institute of Diagnostics and Vaccine Development in Infectious Diseases, State Key Laboratory of Molecular Vaccinology and Molecular Diagnostics, Xiamen University, Xiamen, P. R. China. [3]Department of Respiratory Medicine, Children's Hospital of Chongqing Medical University, Chongqing, P. R. China. [4]These authors contributed equally: Yongpeng Sun, Liqin Liu, Hongsheng Qiang, Hui Sun, Yichao Jiang, Luo Ren, Zemin Jiang. ✉e-mail: emliu186@126.com; abing0811@xmu.edu.cn; zhengzizheng@xmu.edu.cn; nsxia@xmu.edu.cn

results from phase 3 trials of its RSV vaccine for adults over 60[7]. However, the development of a pediatric vaccine has been hindered by the complexity of infants and children's immune system and concerns regarding vaccine enhanced respiratory disease (ERD), underlining the urgent need for effective protection strategies against RSV for children and infants, especially in their first months of life.

Maternal vaccination and the administration of RSV F-specific antibodies to infants are recognized as viable passive immunization approaches to safeguard them from RSV infection[8]. For effective protection, infants require the efficient transplacental transfer of RSV-specific maternally derived antibodies. Nevertheless, these maternally derived antibodies have a relatively short half-life in neonates and decrease significantly over time[9–12], typically offering protection for only up to three months. This duration leaves infants at risk of RSV disease during much of the vulnerable season. In 2019, Novavax's phase 3 clinical trial of its maternal RSV vaccine candidate, ResVax, failed to meet its primary objective[13]. Additionally, in early 2022, GSK discontinued its investigational maternal RSV vaccine, RSVPreF3, in the GRACE phase 3 trial (NCT04605159) due to safety concerns[14]. Meanwhile, Pfizer's ABRYSVO received FDA approval, marking it as the inaugural and sole maternal immunization for newborns up to six months. Despite its approval, concerns were raised by several FDA advisers regarding heightened instances of preterm births among vaccinated women, leading to requirement for stringent post-marketing surveillance to monitor these issues closely[15].

Passive immunization through RSV F-specific neutralizing antibodies (nAbs) stands as a well-established and desirable strategy to protect infants against RSV infection. The RSV F glycoprotein is known to possess at least six antigenic sites[16,17], with sites Ø and V, recognized by the representative nAbs, D25[18] and hRSV90[19] respectively, exclusive to the pre-fusion configuration of F proteins. The remaining sites (sites I, II, III and IV) present on both pre-fusion and post-fusion (post-F) states and are recognized by various other representative antibodies such as 131-2a[20], palivizumab[21], MPE8[22] and 101F[23]. Among these, palivizumab (Synagis®, Sobi) is the first FDA-approved RSV prophylactic for limited use in high-risk infants and young children, leaving most infants out of protection[24,25]. The practical and cost constraints limit its wider application. In contrast, the recently approved nirsevimab, optimized from D25 and targeting site Ø, offer potent, extended protection with a single dose covering the typical RSV season duration[26]. Nirsevimab is anticipated to prevent three times as many RSV events as Pfizer's maternal vaccine ABRYSVO with a superior safety profile[27]. Nonetheless, the targeted antigenic site Ø's low conservation raises concerns about potential immune evasion[18,28], as evidenced by the identification of two nirsevimab-resistant RSV strains with residue substitutions at site Ø in phase trial[29]. Furthermore, some RSV B strains, for instance, B18537, exhibit resistance to nirsevimab's precursor, D25[30–33]. Recent findings also highlight a discrepancy between in vitro and in vivo efficacies of nirsevimab[34]. Motavizumab, a second-generation antibody developed from palivizumab through affinity maturation, also demonstrated the phenomenon of increased in vitro potency without corresponding in vivo efficacy. Despite with increased neutralization potency, motavizumab showed no significant improvement over palivizumab in clinical efficacy and was linked to adverse skin reactions[35–37]. These observations underline that an antibody's increased efficacy and neutralization capability do not necessarily translate to enhanced in vivo antiviral efficacy, emphasizing the need for nAbs targeting universally conserved epitopes across RSV subgroups.

In this study, we characterized a nAb termed 5B11 against RSV, which showed potent and balanced neutralizing efficacy against both RSV-A and -B subgroups. Cryo-electron microscopy (cryo-EM) structures, combined with escape mutant selection, demonstrated that 5B11 targeted a highly conserved and immunologically tolerant epitope within site V, surpassing nirsevimab in comparison. Moreover, in vivo prophylaxis assays indicated that 5B11 necessitated merely one-tenth the dose of 1129 to potently neutralize two RSV subgroups and exhibited a superior capability to prevent B18537 infection than nirsevimab. Therefore, nAb 5B11 emerges as a credible and potent alternative for passive antibody therapeutics. These findings provide vital insights into complementing and comprehending conserved RSV epitopes and are instrumental in guiding the development of antibody drugs, as well as facilitating the rational design of prophylaxis and vaccines against RSV infection.

Results

5B11 is a prefusion-specific, potent and broad nAb

We effectively isolated a murine hybridoma cell specific to RSV, designated 5B11, from mice immunized using a previously reported strategy[38]. The binding capacities of 5B11 to the pre-F (DS-Cav1) and post-F proteins were assessed through an indirect enzyme-linked immunosorbent assay (ELISA), revealing that 5B11 exclusively bound to the pre-F, with half-maximal effective concentration (EC_{50}) of 25.49 ng/mL and 36.82 ng/mL for A2 and B18537 strains, respectively, confirming its specificity for the pre-F (Fig. 1a, b). The binding affinities of 5B11 to DS-Cav1s of A2 and B18537 were identified by surface plasmon resonance (SPR), which revealed the sub-nanomolar affinity of 5B11 to both DS-Cav1 proteins (Fig. 1c, d). Additionally, a humanized version of 5B11 (named h5B11) was generated by mutating amino acids in the framework regions of its heavy and light chain variable domains based on human germline genes with the highest homology (IGHV7-4-1*02 and IGKV-NL1*01) (Fig. S1). h5B11 maintained comparable binding activities to its murine counterpart (Fig. 1a, b).

The neutralization potency of both 5B11 and h5B11 against representative laboratory strains of RSV-A and RSV-B subgroups (including strains A2, Long, B9320 and B18537) was determined through plaque reduction neutralization assays, showing IC_{50} values ranging from 2.22 to 10.75 ng/mL for 5B11, and 2.19 to 9.33 ng/mL for h5B11 (Fig. 1e–h). Comparatively, nirsevimab, which has been proved display approximately 4-fold enhanced in vitro neutralizing activity over its precursor D25 against B18537[19,26,30,32]. We found that nirsevimab could effectively neutralize A2, Long and B9320, with comparable potencies (IC_{50}: 1.79–4.61 ng/mL) to that of 5B11. However, nirsevimab with a threefold decreased potency against B18537 (IC_{50}: 28.49 ng/mL) compared to 5B11 (Fig. 1e–h). Notably, in a previous study, we identified antibody 5C4 poorly neutralizing subtype B strains when neutralizing the representative RSV B laboratory strain, B18537[39]. In contrast, the control nAbs palivizumab and its murine precursor 1129, demonstrated significantly lower neutralization capacities and exhibited approximately 20- to 30-fold less potent neutralizing capacity (IC_{50}: 112.30 to 217.0 ng/mL) (Fig. 1e–h).

To comprehensively investigate the neutralization breadth of the aforementioned nAbs, a panel of 25 RSV clinical isolates (15 RSV-A and 10 RSV-B, the aligned F protein sequences are included in Supplementary Data 1) was used for further neutralization evaluation. Impressively, 5B11 could effectively neutralize all tested RSV-A and -B isolates with geometric mean IC_{50} of 9.43 ng/mL (range 3.44–21.41 ng/mL) and 14.45 ng/mL (range 2.13–37.30 ng/mL) respectively, which was equivalent to that of nirsevimab and ~30-fold greater than that of 1129 or palivizumab (Fig. 1i). In conclusion, these findings confirm 5B11 as a highly effective and broadly nAb with balanced neutralizing potencies against both RSV-A and -B subgroups.

To investigate the neutralizing mechanism of 5B11, RSV attachment and fusion inhibition assays were performed to evaluate its capacity of inhibiting RSV attachment to cells or virus-to-cell fusion, which clearly demonstrated that 5B11 potently inhibited viral entry by disrupting membrane fusion rather than cell-surface attachment (Figs. 1j, k and S2), similar to the previously reported nAbs D25 and 5C4[18].

https://doi.org/10.1038/s41467-024-54384-x

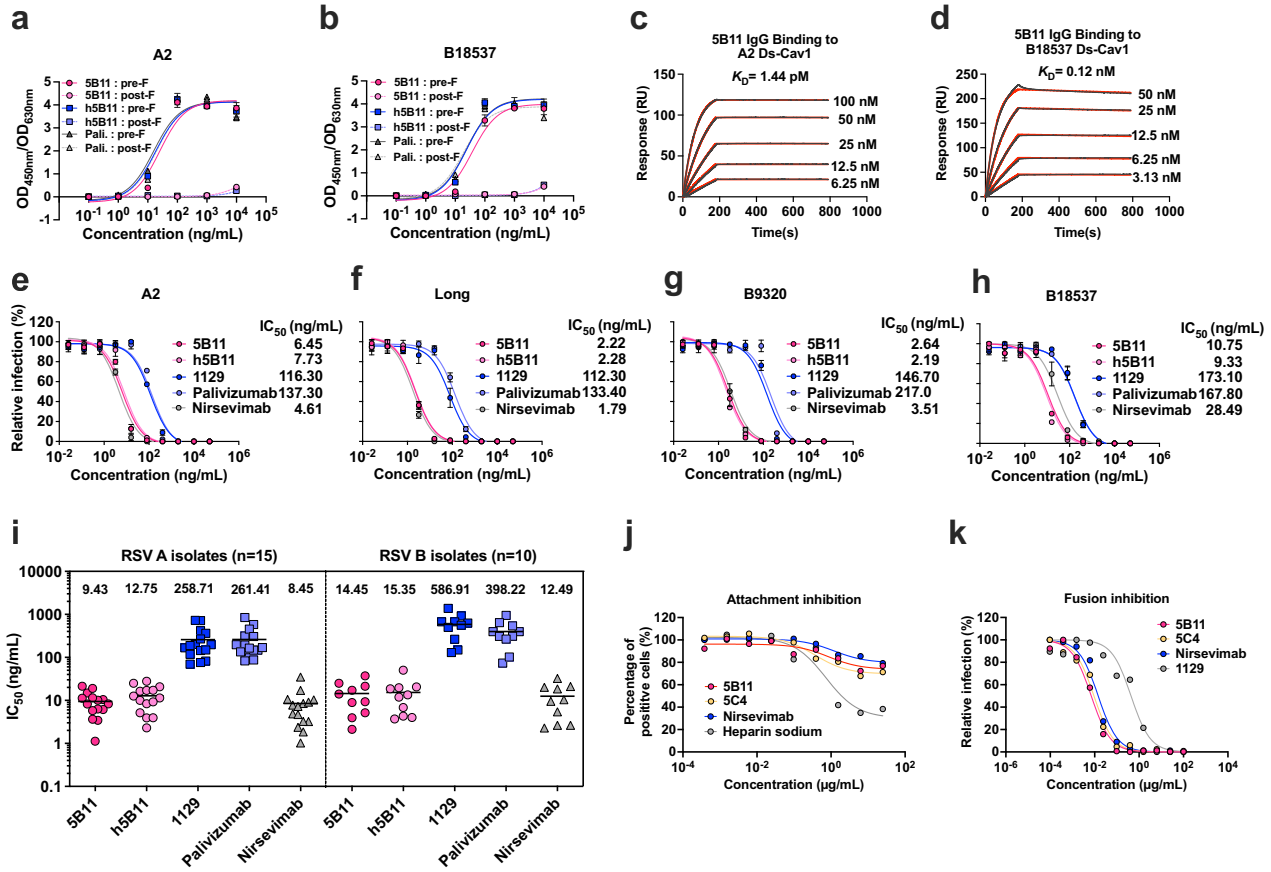

Fig. 1 | In vitro characterization of antibody 5B11. a–d The binding activity of 5B11 to the purified recombinant pre-F (DS-Cav1) and post-F from RSV A2 (**a**) and RSV B18537 (**b**) was measured by indirect ELISA. Data represents one of three independent experiments, shown as mean ± standard deviation (SD) of three technical replicates. Palivizumab (Pali.) was used as a positive control. EC_{50} (ng/mL) was calculated to assess the binding potency of 5B11 with RSV F protein. The binding affinities of 5B11 with RSV-A (**c**) and -B (**d**) DS-Cav1s were identified by surface plasmon resonance (SPR). **e–i** Neutralizing potency of RSV nAbs were measured by RSV plaque reduction neutralization assay and determined by IC_{50} values (ng/mL), which indicated the concentration of nAbs required for reducing 50% of viral infection. Neutralization activities of 5B11 (strawberry), h5B11 (carnation), 1129 (blueberry), palivizumab (orchid) and nirsevimab (aluminum) against RSV laboratory strain A2 (**e**), Long (**f**), B9320 (**g**) and B18537 (**h**) were determined, respectively. Data represents one of three independent experiments, shown as mean ± SD of two technical replicates. **i** A panel of 15 RSV-A ($n = 15$) and 10 RSV-B clinical isolates ($n = 10$) was also tested in the neutralization assay. Data represents one of three independent experiments. Horizontal bars in (**i**) indicate geometric mean IC_{50}. **j**, **k** Attachment inhibition (**j**) and fusion inhibition assays (**k**) for 5B11 and other RSV F-specific antibodies. In the attachment inhibition assay, heparin sodium served as a positive control. Data in (**j**) and (**k**) are representative of three independent experiments. Source data are provided as a Source Data file.

Cryo-EM analysis of 5B11 binding to the pre-F protein

To structurally elucidate the broad neutralization mechanism of 5B11, we prepared the prefusion-stabilized glycoprotein F variants, DS-Cav1 and sc9-10 DS-Cav1, from RSV A2 and B18537 strains, following previously established protocols[40,41]. We then prepared immune complexes by mixing the antigen-binding fragments (Fabs) of 5B11 with two kinds of pre-F proteins respectively (Fig. S3a–d). High-performance liquid chromatography (HPLC) analysis confirmed that 5B11 bound to both A2 and B18537 pre-F proteins (Fig. S3e, f). Cryo-EM structural determination of A2 DS-Cav1:5B11 and B18537 sc9-10 DS-Cav1: h5B11 achieved resolutions of 3.19 Å and 3.51 Å, respectively (Figs. 2a–e, S4, S5 and Table S1). The electron density maps clearly revealed the recombinant pre-F proteins and 5B11 Fab components with the pre-F trimer displaying a lollipop-like conformation marked by tightly entwining of three protomers around a threefold axis of symmetry (Fig. 2a, b, d). Each 5B11 Fab engaged a single protomer laterally, resembling a propeller from a top-down view (Fig. 2b). Each Fab interacted exclusively with a single protomer, indicating that 5B11 targets individual protomers rather than the trimer as a whole. Moreover, a structural comparison of A2- and B18537-derived pre-F forms demonstrated a high degree of similarity in the prefusion conformation (Fig. S6), underscoring the structural conservation of the F proteins across subtypes.

We next performed the localized refinements of both complexes to improve the resolution of the antibody interface regions, resulting in localized density maps with resolutions of 3.13 Å for A2 DS-Cav1:5B11 and 3.32 Å for B18537 sc9-10 DS-Cav1:h5B11 (Figs. S4, S5 and Table S1). The improved resolutions facilitated accurate model building and enabled the identification of the precise epitope of 5B11 on the pre-F proteins. 5B11 extensively interacts with A2- and B18537-derived pre-F proteins by burying surface areas of about 893 $Å^2$ and 907 $Å^2$, respectively (Fig. 2f, g and Table S1). The epitope residues of A2- and B18537-derived pre-F proteins exhibited significant similarity, primarily composed of a helix (α3)-sheet (β3)-loop motif. A total of 13 residues (A2: E161, G162, N165, K166, K168, S169, L172, V179, S180, S182, K196, E294, E295) and 14 residues (B18537: N63, K65, E161, G162, N165, K166, K168, N169, L172, V179, S180, K196, E294, E295) from the two subtypes of pre-F proteins participate in the interaction to 5B11, respectively. Of these residues,12 are identical (Fig. 2f, g).

Numerous RSV neutralizing antibodies targeting diverse neutralizing-sensitive epitopes on the pre-F have been reported, with six binding sites currently characterized (Fig. S8)[17]. We next

https://doi.org/10.1038/s41467-024-54384-x

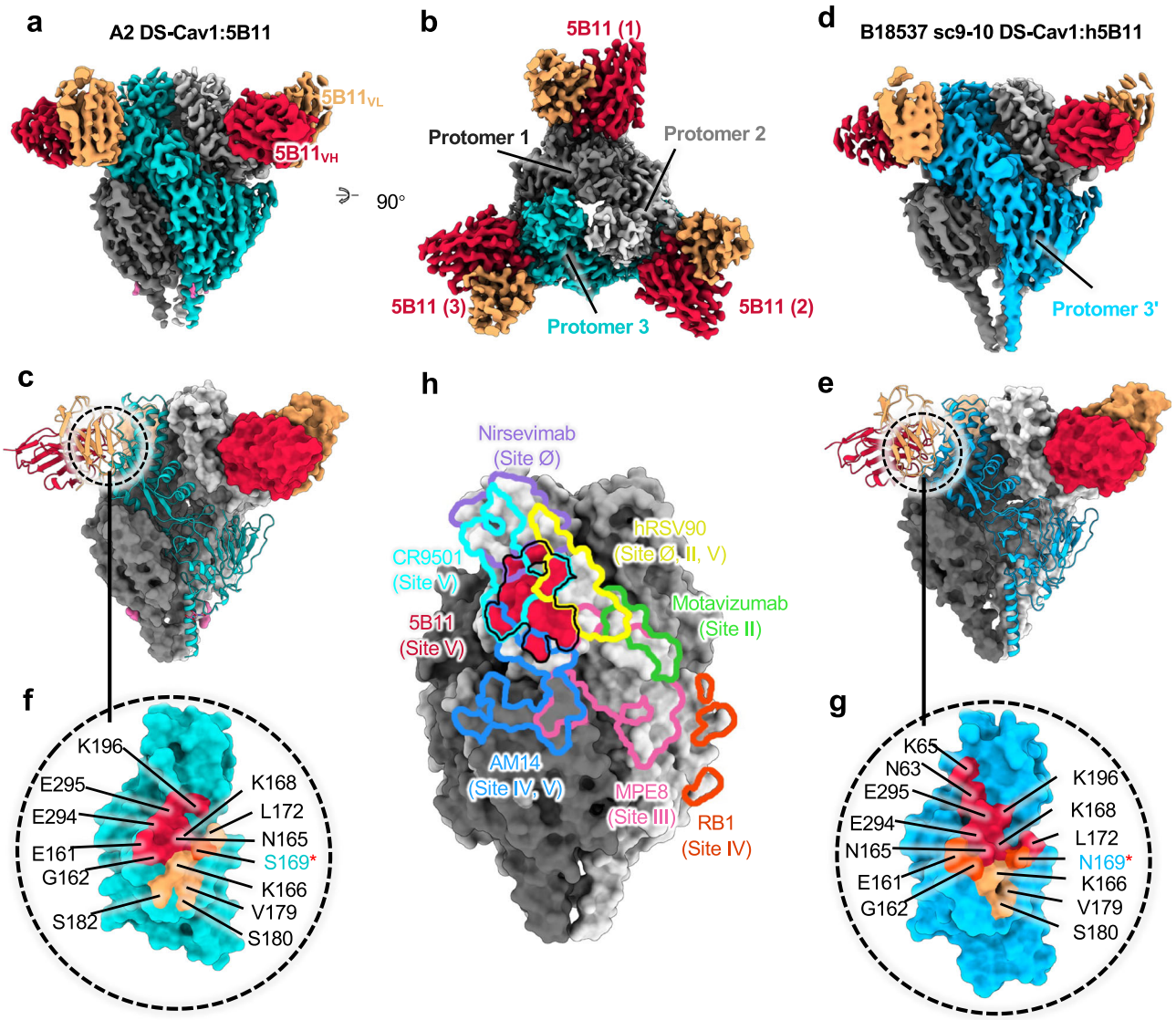

Fig. 2 | Cryo-EM structures of 5B11 bound RSV A2 and B18537 DS-Cav1s. **a**, **b** Cryo-EM density maps of the A2 DS-Cav1:5B11 complex viewed from side view (**a**) and top view (**b**). The pre-F trimer is colored in dark gray (protomer 1), light gray (protomer 2), and turquoise (protomer 3), respectively. Each 5B11 fab is bound to one protomer, and the density of light and heavy chain of 5B11 are colored in crimson and sandy brown, respectively. The glycans density on pre-F are shown in pink. **c** Atomic model of A2 DS-Cav1:5B11 is presented as a surface representation, with one protomer and the 5B11 Fab shown in cartoon representation. The decorated glycans on A2 DS-Cav1 are depicted as pink sticks and surface. **d**, **e** Cryo-EM density maps of B18537 sc9-10 DS-Cav1: h5B11complex viewed from side view (**d**). The atomic model of B18537 sc9-10 DS-Cav1: h5B11 is also presented as cartoon and surface representation. To distinguish from A2 pre-F, protomer 3′ is colored deep sky blue. **f** The epitope comparison of 5B11 with seven other previously published antibodies: nirsevimab (site Ø, purple line), palivizumab (site II, green line), MPE8 (site III, pink line), RB1 (site IV, brown line), CR9501 (site V, cyan line), hRSV90 (site VIII, yellow line) and AM14 (blue line) on A2 pre-F trimer. The 5B11 epitope is highlighted in red and depicted with black solid lines. **g**, **h** Surface mapping of the 5B11 epitope on A2 DS-Cav1 (turquoise) and B18537 sc9-10 DS-Cav1 (deep sky blue), with the same color as in (**c**) and (**e**). Residues common to the light and heavy chain of 5B11 are colored orange red.

investigated the binding modes of 5B11 on DS-Cav1 and compared to other reported nAbs. It is observed that the 5B11's epitope partially overlaps with that of CR9501 (site V)[31], hRSV90 (sites Ø, II, V)[19] and AM14 (sites IV, V)[42], but differs from those recognized by nirsevimab (site Ø)[26], palivizumab (site II)[43], MPE8 (site III)[22] and RB1 (site IV)[28] (Fig. 2h). Notably, the 5B11 epitope undergo structural rearrangements during the transition of prefusion to postfusion phase, ultimately stabilized into an extended α5-helix on the post-F[18]. This implies that 5B11 exclusively binds to the pre-F conformation, a finding corroborated by biochemical assays (Fig. 1a, b). Together, these findings underscore that 5B11 targets an epitope within site V on the pre-F, which does not fully align with the epitope profiles of most antibodies reported.

5B11 binds a highly conserved antigenic site

To elucidate the structural basis for the broad neutralization of 5B11, we carried out an in-depth examination of its interaction with both subgroups of the pre-F. The interface between A2 DS-Cav1 and 5B11 comprises a complex array of interactions, primarily including ten hydrogen bonds and one salt bridge (Fig. 3a, b). Notably, the interaction is predominantly mediated by the complementarity determining regions 1 and 3 of the heavy chain (CDRH1 and CDRH3), along with contributions from selected residues from the light chain CDR3 (CDRL3), contributing the binding interface (Fig. 3a). In particular, residue S33 of CDRH1, H35 of framework region 2 (FR2), Y100 and Y101 of CDRH3, and W92 of CDRL3, establish four hydrogen bonds and one salt bridge with the α3-helix of the pre-F ranging from residue E161 to

https://doi.org/10.1038/s41467-024-54384-x

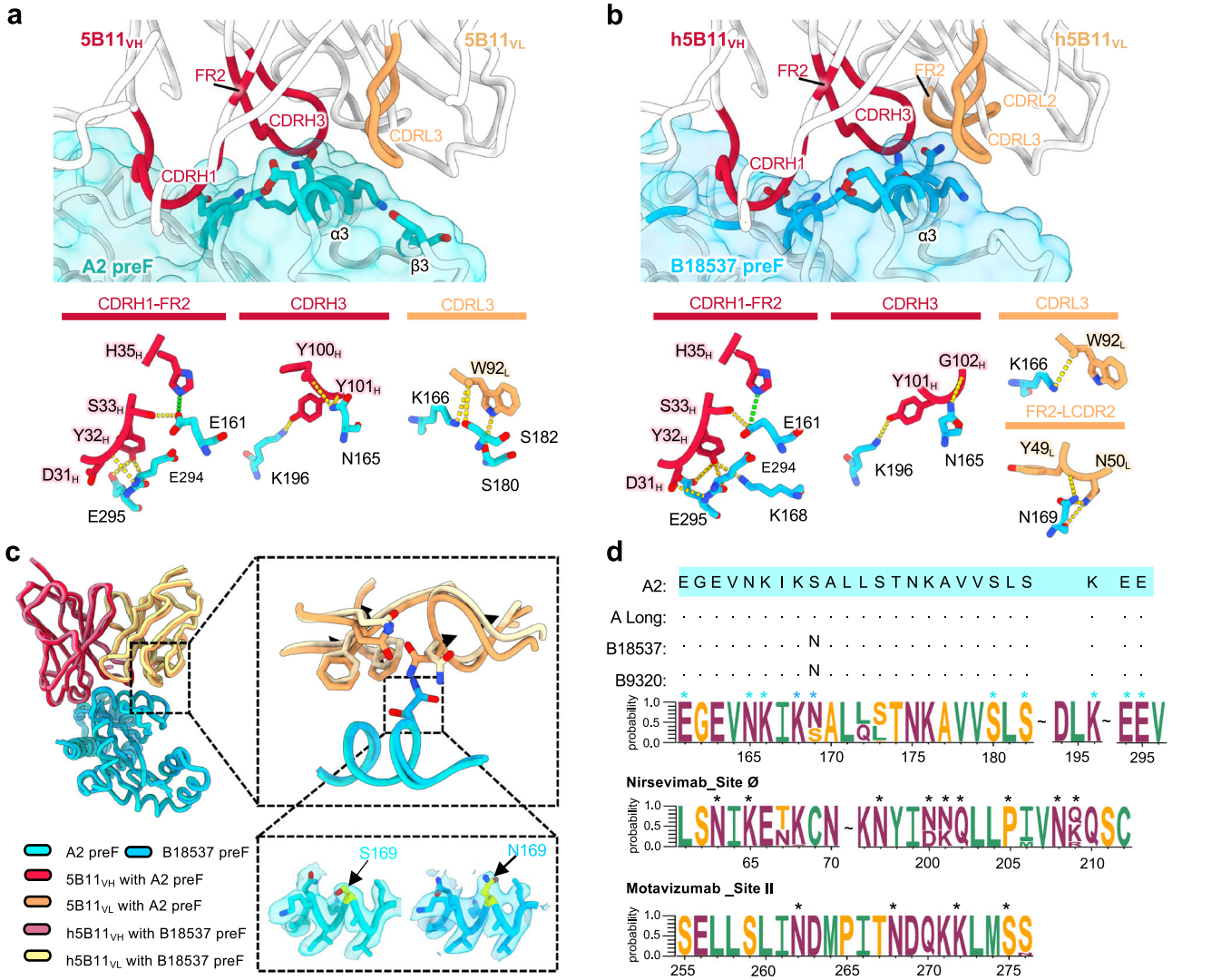

Fig. 3 | 5B11 recognizes a conserved epitope on the RSV pre-F. a The interaction details between 5B11 and A2 DS-Cav1. In the upper panel, antibody 5B11 is shown as a cartoon and colored in white. The CDRH1, CDRH3, and FR2 involved in the interaction are colored in crimson and CDRL3 is colored in orange. The A2 pre-F antigen is shown as cartoon and surface representations and colored in turquoise. In the lower panel, hydrogen bond and salt bridge interactions are shown as yellow and green dashed lines, respectively. The residues involved in hydrogen bond and salt bridge interactions are shown as stick and labeled as indicated. All interactions shown are from the same perspective. **b** The interaction details between h5B11 and B18537 sc9-10 DS-Cav1. The B18537 pre-F antigen is colored in deep sky blue. **c** Structural comparison of the interactions of 5B11:A2 DS-Cav1 and h5B11:B18537 sc9-10 DS-Cav1. Changes in the binding angle of the h5B11 light chain caused by B18537 pre-F N169 are indicated by black dashed arrows. **d** The sequence conservation of 2074 full-length RSV F genes in the last decade downloaded from GenBank. The percent conservation of each amino acid within the binding region was calculated and represented as color-coded bars: Hydrophilic amino acid in purple, Neutral amino acid in orange, Hydrophobic amino acid in green. F sequences of RSV A2, A Long, B18537, B9320 with highlighted footprint of 5B11. Simultaneously shows the sequence conservation of nirsevimab and palivizumab antibody epitopes.

L172 (Fig. 3a). In addition, a substantial number of van der Waals contacts are formed between 5B11 and this region. The CDRH1 residues D31 and Y32 also form three hydrogen bonds with an adjacent loop comprising amino acids 294 and 295 of the pre-F. Furthermore, the CDRL3 of 5B11 interacts with S180 and S182 of the β3 region creating two more hydrogen bonds.

The binding of 5B11 to B18537 pre-F mirrors its interaction with A2 pre-F (Fig. 3b). Among the 14 epitope residues, only residue 169 exhibits variation between the two subtypes of pre-F proteins (A: S169; B: N169). However, this single amino acid variation does not affect the binding or neutralizing activity of 5B11. Interestingly, the longer side chain of N169 in subtype B seems to enhance its interaction to the light chain of 5B11, resulting in a larger buried surface area with B18537 pre-F. Correspondingly, LCDR1 formed three additional hydrogen bonds with residues N169 in the α3 (Fig. 3b). However, it should be noted that, structurally, the longer side chain of N169 in the subtype B pre-F would push the light chain of 5B11 away from its binding site to some extent (Fig. 3c), which might explain the variation in neutralizing efficacy of 5B11 against two subtypes of viruses. Nevertheless, despite the variation at residue 169 (S/N) between the two subtypes, 5B11 consistently forms similar interactions across both subtypes, thereby exhibiting comparable neutralizing effectiveness.

To assess the evolutionary conservation of the 5B11-binding site, we conducted a sequence alignment of a total of 2074 full-length genes of RSV F proteins deposited in GenBank over the past decade (subtype A: 724; subtype B: 1350). Sequence analysis unveiled that most of the amino acids within the 5B11 epitope are highly conserved across all analyzed RSV A and B subtypes, with the exception of residue 169, which appears as serine in 35% and asparagine in 65% of the sequences (Fig. 3d). As previously mentioned, amino acid variation

https://doi.org/10.1038/s41467-024-54384-x

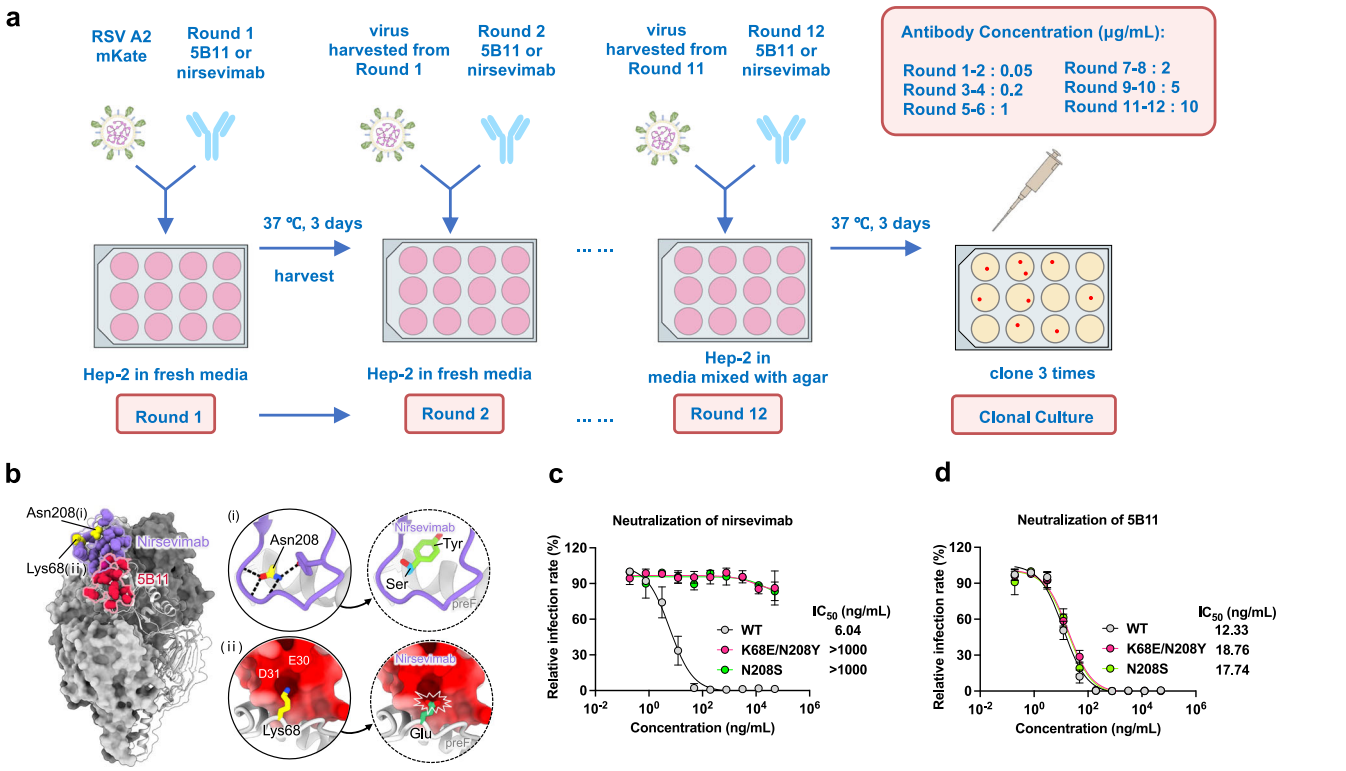

Fig. 4 | Resistant mutant isolation under the pressure of 5B11 and nirsevimab. **a** Schematic of the resistant mutant selection process. **b** Mapping amino acid substitutions of nirsevimab-resistant mutants on the pre-F protein (PDB ID: 5UDC). The binding epitopes of nirsevimab and 5B11 are depicted in purple and red, respectively, with the overlapping residues in magenta. Yellow residues indicate the positions of escape mutations (Asn208 (i) and Lys68 (ii)). **(i)** Interaction details between nirsevimab and Asn208 on the pre-F (left circle), and the hypothetical structures for substitution N208Y or N208S (right circle). The black dashed lines indicate hydrogen bonds. **(ii)** Electrostatic interaction between nirsevimab and Lys68 on the pre-F, and the hypothetical structure for substitution K68E (right circle). The surrounding residues interacting with Lys68 on the pre-F are highlighted in red according to the Coulomb electrostatic potential, indicating a negative charge. Lys68 is positively charged, while Glu is negatively charged. **c**, **d** The susceptibility of nirsevimab-resistant mutants to the neutralization of nirsevimab (**c**) and 5B11 (**d**) was evaluated by RSV neutralization assay. Data represents one of three independent experiments, shown as mean ± SD of three technical replicates. Source data are provided as a Source Data file.

between subtypes at position 169 does not compromise the neutralizing prowess of 5B11, highlighting its targeting of a highly conserved antigenic site. In contrast, the epitope recognized by nirsevimab (site Ø) is less conserved, exhibiting high-frequency mutations at two positions 206 and 209, including one key residues (position 209) (Fig. 3d). Another approved nAb, palivizumab, shows high conservation of its epitope residues (site II), albeit with a relatively lower neutralizing efficacy. Overall, these observations underline the profound conservation of the critical residues involved in 5B11 binding and provide insights into the molecular basis behind its broad neutralization capacity.

5B11 demonstrates resilience against RSV mutational escape

To evaluate the conservation and immunological tolerance of the 5B11-binding site, resistant mutant screening was performed by using 5B11 and nirsevimab, respectively (Fig. 4a). Following 12 rounds of in vitro selection under pressure, no mutant resistant exclusively to 5B11 was detected, even subjecting the virus to a final concentration of 10 μg/mL of 5B11, indicating its potent and broad activity. Conversely, two nirsevimab resistant mutants emerged after the virus was equivalently subjected to a final antibody pressure of 10 μg/mL. Genetic sequencing of these mutants' F genes uncovered two types of amino acid substitutions within the nirsevimab-binding site: K68E/N208Y and N208S (Fig. 4b). Structural analysis revealed that the asparagine (N) at position 208 in the F proteins of both RSV A and B subtypes makes polar contacts with nirsevimab, mediated by side-chain interactions (Fig. 4b). Altering asparagine at this position to either tyrosine (Y) or serine (S) markedly diminishes nirsevimab's binding efficiency, impacting viral evolution[26]. Additionally, the mutation from lysine (K) at position 68 to glutamic acid (E), which introduces a charge reversal, is likely to interfere with nirsevimab's binding due to electrostatic repulsion (Fig. 4b). Further investigation using an RSV neutralization assay confirmed the resistance of these two mutants against nirsevimab, exhibiting complete neutralization evasion (Fig. 4c), yet they remained sensitive to 5B11 (Fig. 4d). These findings underscore the superior resilience and broader neutralizing capacity of 5B11 against RSV, highlighting its potential as a more robust therapeutic option compared to nirsevimab in circumventing viral escape through mutation.

Prophylactic and therapeutic efficacy of 5B11 in RSV-infected rodent models

We next proceeded to assess the in vivo prophylactic and therapeutic efficacy of 5B11 against RSV infection. Given that B18537 escaped from both D25 and 5C4, this strain was selected as the representative strain of RSV B subgroup, and along with A2 strain, were used to challenge in a cotton rat or mouse model. Firstly, the prophylactic efficacy of the murine antibody 5B11 compared to the control antibody 1129, using both low (1.5 mg/kg) and high doses (15 mg/kg), was performed. Each antibody was cloned into the pVRC8400 vector, featuring an identical murine IgG2a subclass backbone. Animals were intramuscularly injected with either the low or high dose of 5B11 or 1129 one day before being challenged with RSV, whereas the control group received PBS. 24 h after antibody administration, all animals were anesthetized and

https://doi.org/10.1038/s41467-024-54384-x

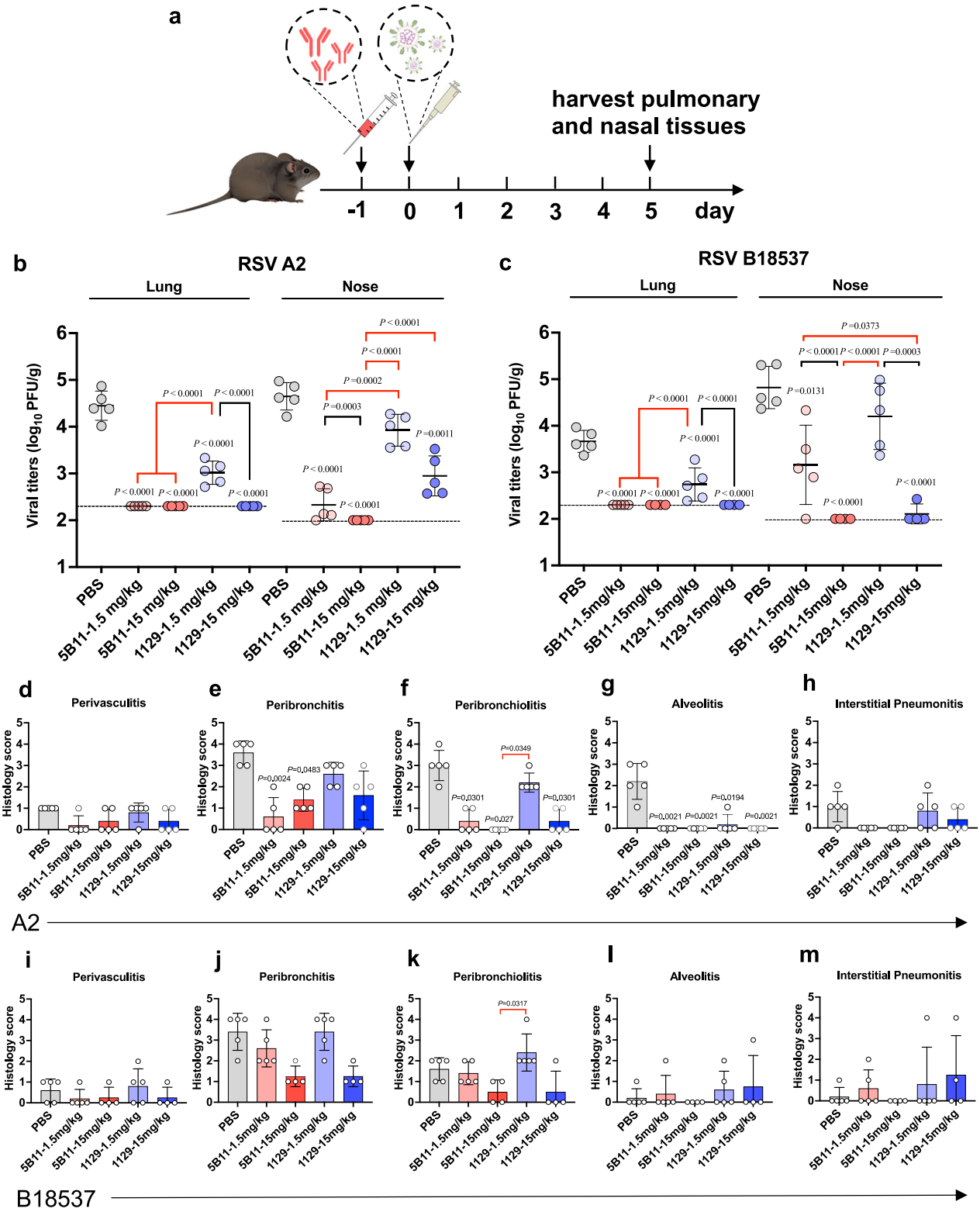

infected intranasal with strains A2 or B18537. Five days post-infection, nasal and lung tissues from cotton rats were collected for viral titers and pulmonary histopathology assessment (Fig. 5a).

Virus titration analysis showed that high-dose 5B11 effectively prevented RSV-A and -B infection in both the upper (nasal turbinates) and lower (lungs) respiratory tracts, achieving complete inhibition of viral replication to undetectable levels (Fig. 5b, c). Low-dose 5B11 also fully inhibited viral replication in the lungs and significantly reduced viral titers in the nasal turbinates—209-fold for A2 and 46-fold for B18537—compared to the PBS-treated controls (Fig. 5b, c). In contrast, 1129 at high dose could only suppress viruses in lungs and failed to reduce viral loads in the upper airways either in its low- or high-dose (Fig. 5b, c), mirroring its prophylactic efficacy in the Balb/C mouse model against RSV A2 infection[38].

Additionally, histopathological analysis of the lungs revealed that both doses of murine 5B11 effectively alleviated pulmonary inflammation induced by RSV infections (Figs. 5 and S9). In experiments aimed to preventing A2 infection, animals receiving a high dose of 5B11

Fig. 5 | Prophylactic efficacies of 5B11 against RSV A2 and B18537 infections in cotton rat model. a The schematic diagram for RSV prophylaxis assay. **b** RSV titers in lungs and noses in each group of cotton rats five days after exposure to 2×10^6 pfu of RSV A2. Five animals were used per group ($n = 5$). **c** RSV titers in lungs and noses in each group of cotton rats five days after exposure to 4.8×10^5 pfu of RSV B18537. Four to five animals were used per group ($n = 4$–5). Error bars represent mean values with SD. The dotted line means the limit of detection. Statistical differences between groups were analyzed by one-way ANOVA, followed by Tukey's multiple comparisons post hoc test. **d**–**m** Lung histopathology was quantitatively analyzed by a pathology scoring system in animals prophylactically inoculated by PBS and RSV F antibodies. Histology scores of cotton rats infected with RSV strain A2 (**d**–**h**) and B18573 (**i**–**m**) were respectively shown for the prophylactic evaluation of 5B11 and 1129 at 1.5 mg/kg and 15 mg/kg. Blood vessels (perivasculitis; **d** and **i**), bronchus (peribronchitis; **e** and **j**), bronchioles (peribronchiolitis; **f** and **k**), alveolar lumen (alveolitis; **g** and **l**) and lung interstitium (interstitial pneumonitis; **h** and **m**) in lung tissues were scored ranging from 0 to 4 points, according to the number of layers of inflammatory cells. Error bars represent mean values with SD. Kruskal-Wallis test was used for statistical differences between groups and corrected for multiple comparisons using Dunn's method. Source data are provided as a Source Data file.

exhibited only minimal peribronchitis, manifested as slight infiltration of inflammatory cells around the bronchi (Figs. 5e and S9a). As for B18537 infection, both peribronchitis and mild peribronchiolitis were observed in animals treated with low dose of 5B11 (Figs. 5j, k and S9b). Notably, no evidence of perivasculitis, peribronchiolitis, alveolitis, or interstitial pneumonitis was observed in any 5B11-treated groups across both sets of prophylactic experiments (Fig. 5d–m). In contrast, the control nAb 1129 exhibited mild peribronchitis in the high-dose group, while its low dose resulted in severe peribronchitis and peribronchiolitis, along with bronchial and bronchiolar wall thickening and significant infiltration of inflammatory cells in all tested scenarios (Figs. 5e, f, j, k and S9a, b). Taken together, these results suggest 5B11's superior capacity to suppress pulmonary inflammation, with the efficacy of low-dose 5B11 paralleling that of high-dose 1129.

Despite the controversy surrounding the feasibility of RSV neutralizing antibodies as RSV therapeutics, we still attempted to evaluate the potential of 5B11 as a therapeutic agent in Balb/C model. Animals were administrated with high (15 mg/kg) or low doses (5 mg/kg) of 5B11 or 1129 one day after inoculation with RSV A2 (2×10^6 PFU per animal) (Fig. 6a). RSV plaque assays for lung and nasal tissues harvested at 5 dpi demonstrated complete elimination of viral loads in the lungs across all four antibody groups (Fig. 6b). Viral titers in the nasal turbinates were nearly undetectable (Fig. 6c). Lung pathological assessments revealed clear and intact blood vessels, bronchus, bronchioles and alveolar lumen in lung tissues of animals from high-dose 5B11 group, along with only a slight infiltration of inflammatory cells. This suggests that high-dose 5B11 effectively mitigated pulmonary inflammation, particularly alveolitis and interstitial pneumonitis (Fig. 6d–i). In contrast, neither low-dose 5B11 nor 1129 at two doses significantly reduce pulmonary inflammation levels. High-dose 1129 only exerted a notable relief effect on interstitial pneumonia (Fig. 6d–i). These findings demonstrate the great potential of 5B11 at high doses for RSV treatment.

We next explored the prophylactic capabilities of humanized 5B11 (h5B11) as an antibody candidate against RSV infection. A parallelly comparative analysis with palivizumab and nirsevimab using a low dose (1.5 mg/kg) were conducted in the cotton rat model, as described above (Fig. 5a). Consistent with its in vitro neutralization efficacy, h5B11 demonstrated excellent antiviral activity, outperforming palivizumab and matching nirsevimab in thwarting A2 strain infections (Fig. 7a, c–g). Regarding A2 strain exposure, h5B11 eradicated viral replication in the lungs and achieved an approximate 80-fold (1.9 logs) reduction in viral titers in nasal turbinates. Similarly, nirsevimab prevented lung viral infection entirely and diminished viral titers in nasal turbinates by about 125-fold (2.1 logs), consistent with the reported prophylactic effectiveness of 1–2 mg/kg of MEDI8897 (nirsevimab) in the cotton rat model[26]. However, low-dose palivizumab offered limited protection, reducing viral loads by approximately 20-fold in the lungs and 4-fold in nasal turbinates (Fig. 7a), echoing earlier findings[26,30]. Pulmonary histopathology implied that h5B11 was more adept at curtailing pulmonary inflammation than nirsevimab, particularly in lessening alveolitis and interstitial pneumonitis (Figs. 7f, g and S9c).

In the case of B18537 strain, animals treated with h5B11 exhibited a significantly higher antiviral efficacy, achieving approximately a 69-fold (1.84 logs) reduction in pulmonary viral titers compared to the nirsevimab treatment group, which showed about 13-fold (1.13 logs) decrease. h5B11 was also approximately 5-fold (0.71 logs) more effective in reducing viral titers in the lungs than nirsevimab (Fig. 7b). Notably, the h5B11-treated animals displayed no significant infiltration of inflammatory cell or thickening around blood vessels, bronchi, bronchiole, alveoli and lung interstitium, and the alveolar structures (Figs. 7h–l and S9d). While not statistically significant, h5B11 appeared to alleviate peribronchitis, peribronchiolitis and interstitial pneumonitis more effectively than both nirsevimab and palivizumab (Fig. 7i, j, l). In contrast, MEDI8897, while reported to neutralize both RSV B/WV/14617/1985 and B18537 strains effectively, failed to completely inhibit replication of B/WV/14617/1985 in the lungs at a dose of 1 mg/kg[34]. These in vivo findings underline nirsevimab's limited prophylactic efficacy against certain subgroup B virus infections.

Although no previous reports have highlighted the in vivo prevention deficiency of nirsevimab and D25 against B18537, a study by Wen et.al. [34] revealed nirsevimab's reduced neutralizing activity against B18537 compared to RSV subgroup A strains, consistent with our results (Fig. 1). Furthermore, D25 was also reported with weaker neutralizing potency against several RSV-B strains, including B18537[30–33]. To explore the underlying mechanism behind the reduced in vivo prevention of nirsevimab against B18537 infection, we initially assessed its binding to the pre-F and post-F proteins from strain A2 and B18537, respectively, via ELISA, finding significantly weaker binding to B18537 pre-F compared to A2 pre-F (Fig. S10a, b). Subsequent SPR analysis confirmed that nirsevimab's much weaker affinity for B18537 pre-F at >800 nM, which is at least 5700-fold weaker than 5B11's 0.124 nM (Fig. S10c, d). Structural and sequential analysis revealed that nirsevimab's reduced binding and antiviral activity against B18537 might be due to a hydrogen bond disruption caused by the longer side chain of arginine at position 202 of B18537 pre-F, which collides with asparagine at position 31 of nirsevimab's light chain (Fig. S10e, f). In summary, these observations indicate that 5B11 possesses potent in vivo antiviral efficacy against both RSV-A and -B infection, offering superior prophylactic benefits against RSV B18537 compared to nirsevimab.

The in vivo EC_{50} of h5B11 were also evaluated in the cotton rat model, employing a serial threefold dilution of the antibody across doses ranging from 3 mg/kg to 0.033 mg/kg. This protocol incorporated five dosage titers: 3 mg/kg, 1 mg/kg, 0.33 mg/kg, 0.11 mg/kg and 0.033 mg/kg. Subsequent to antibody administration, serum samples were collected 24 h later for antibody concentration analysis, which was followed by an intranasal challenge using either RSV strain A2 or B18537. Five days post-challenge, nasal and lung tissues were collected for the evaluation of viral loads. The analysis illustrated that h5B11 manifested EC_{50} values of 2.14 μg/mL against RSV A2 and 3.98 μg/mL against B18537 in the lungs (Fig. 7m, o). While in the upper respiratory tract (nasal turbinates), the EC_{50} values were 19.80 μg/mL against A2 and 22.82 μg/mL against B18537 (Fig. 7n, p). These results confirmed that h5B11 provided potent, dose-dependent antiviral efficacy in both the upper and lower respiratory tracts post RSV infection and demonstrated comparably effective activity against both RSV-A and RSV-B subtypes.

https://doi.org/10.1038/s41467-024-54384-x

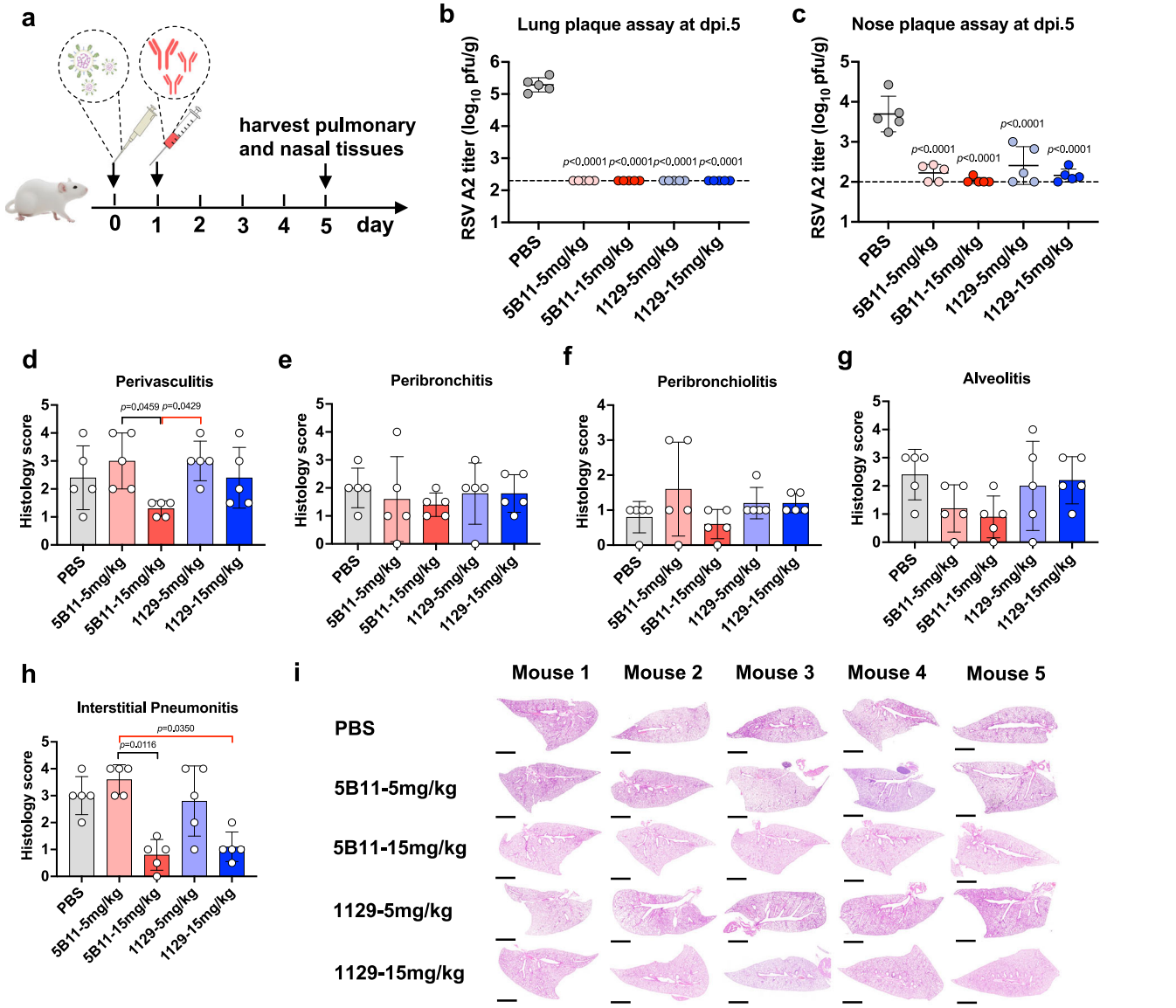

Fig. 6 | Therapeutic efficacy of 5B11 in RSV-infected Balb/C mice. a The schematic diagram for RSV therapeutic assay. Five animals were used per group ($n = 5$). Balb/C mice were treated intramuscularly with either 5B11 or 1129 at two dosage levels (5 mg/kg and 15 mg/kg) at day 1 post exposure to 2×10^6 pfu of RSV A2. The control group received an injection of PBS. Lung and nasal tissues from each group of mice were harvested at day 5 post-infection. **b**, **c** Viral titers in lungs (**b**) and nasal turbinates (**c**) were measured by RSV plaque assays. The dotted line means the limit of detection. Statistical differences between groups were analyzed by one-way ANOVA, followed by Tukey's multiple comparisons post hoc test. Error bars represent mean values with SD. **d**–**h** Histology scores of lungs in Balb/C mice infected with strain A2. Scale bars: 2 mm. Kruskal–Wallis test was used for statistical differences between groups and corrected for multiple comparisons using Dunn's method. Error bars represent mean values with SD. **i** Histopathological sections of lungs. Histochemical staining of H&E was repeated independently three times and one representative result was shown. Source data are provided as a Source Data file.

h5B11 with the YTE modification exhibits an extended half-life and protects cotton rats against RSV infections

The YTE mutation (M252Y/S254T/T256E) in the fragment crystallizable (Fc) regions of antibodies has been proven to prolong their in vivo serum half-lives[26,44,45]. In this study, the YTE mutation was introduced into the Fc region of antibody h5B11, creating a variant named h5B11-YTE. SPR analysis revealed that h5B11-YTE presented a higher binding affinity for human neonatal FcR (hFcRn) at pH 6.0 than the wild-type h5B11 (h5B11-WT) (Fig. S11a). Pharmacokinetic (PK) profiles in human FcRn transgenic mice confirmed that h5B11-YTE received an extended serum half-life (137.5 h ± 24.2 h) in vivo compared to h5B11-WT, comparable to that of nirsevimab (124.6 h ± 21.4 h) (Fig. S11b). The prophylaxis studies in cotton rat model indicated that the long-acting antibody, h5B11-YTE, retained the protective efficacy of its precursor h5B11 in vivo, exhibited excellent in vivo antiviral activities against both RSV-A and -B infections and possessed a superior capability to prevent B18537 infection when compared to nirsevimab (Fig. S11c–n).

Discussion

Passive immunization with RSV F antibodies presents a safer and effective countermeasure to safeguard infants and children against RSV infections, a strategy also recommended by the WHO. Palivizumab serves as a convincing exemplar which has been successfully applied in clinic over two decades. Since its introduction, various antibodies have progressed to clinical stages. Motavizumab, an enhanced second-generation antibody derived from palivizumab through affinity maturation techniques, exhibits approximately 10-fold more potent than its predecessor[35]. Nonetheless, clinical trials indicated that

https://doi.org/10.1038/s41467-024-54384-x

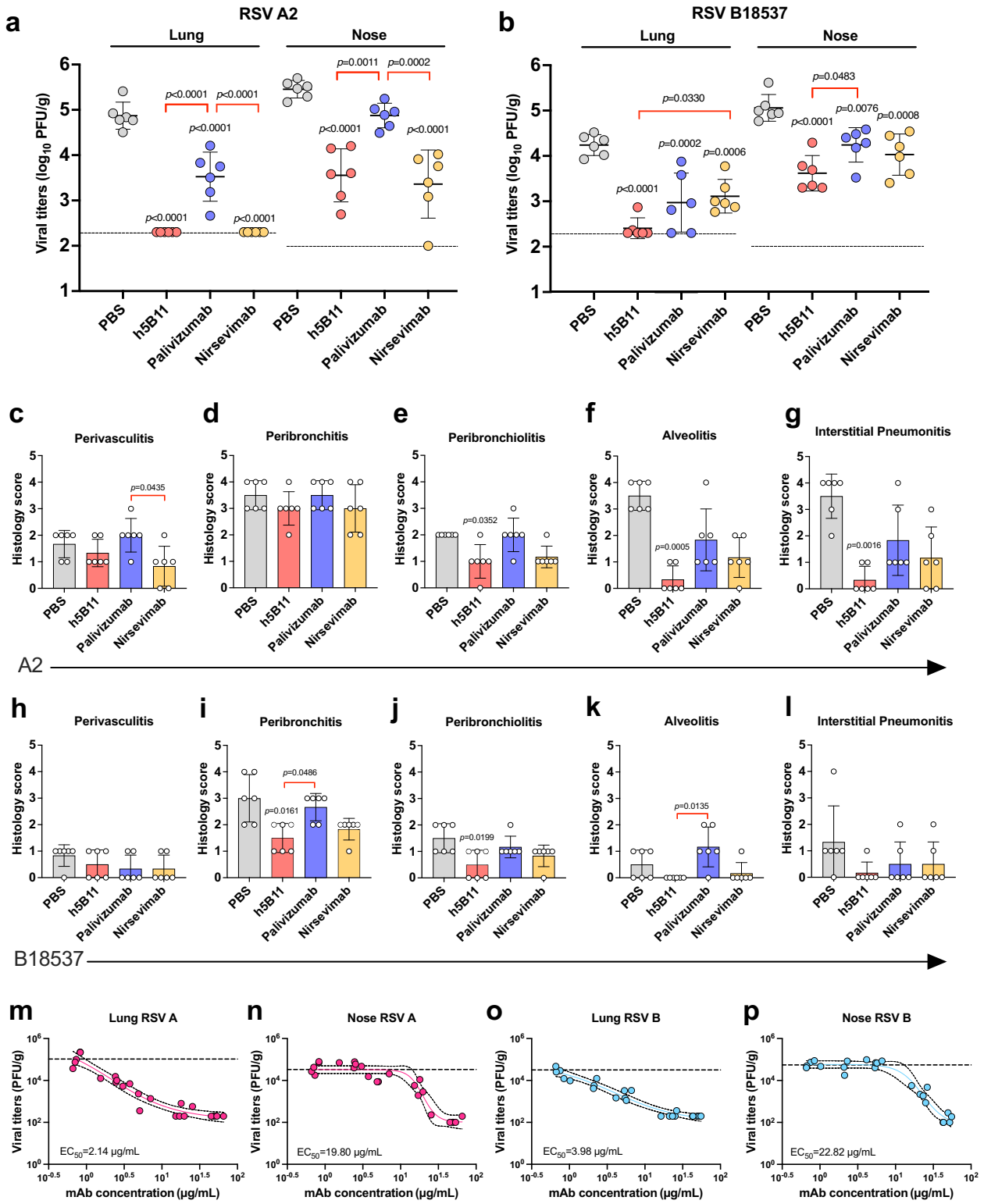

motavizumab did not offer superior efficacy compared to palivizumab and was associated with adverse skin reactions[36,37]. Nirsevimab, an affinity-optimized human nAb developed from its precursor D25, demonstrated approximately 4-fold increase in neutralization capacity for both RSV-A and -B subgroups[26]. It also outperformed D25 in neutralizing RSV B18537 strain, which had shown relatively weaker potency against the same strain[19,30,32]. However, despite its enhanced neutralizing potency, our study uncovered that nirsevimab was less effective than 5B11 in inhibiting virus activity in the lungs of cotton rats challenged with B18537 (Fig. 7b). Nirsevimab exhibited the potent neutralization against B18537, albeit less potent than that against RSV A strains. Nonetheless, our investigations unveiled that nirsevimab's affinity for the B18537 F protein was considerably weaker (Fig. S10), indicating that antibody affinity is more closely aligned its in vivo protection capabilities. Conversely, 5B11 demonstrated high-affinity interactions with the pre-F proteins of both RSV A and B subtypes

Fig. 7 | Prophylactic efficacies of h5B11 against RSV A2 and B18537 infections in cotton rat model. a RSV titers of lungs and noses in each group of animals five days after 2×10^6 pfu of RSV A2 challenge. Six animals were used per group ($n = 6$). **b** RSV titers of lungs and noses in each group of animals five days after 4.8×10^5 pfu of RSV B18537 challenge. Six animals were used per group ($n = 6$). Error bars represent mean values with SD. The dotted line means the limit of detection. Statistical differences between groups were analyzed by one-way ANOVA, followed by Tukey's multiple comparisons post hoc test. **c**–**l** Histology scores of lungs of cotton rats infected with RSV strain A2 (**c**–**g**) and B18573 (**h**–**l**), respectively. Blood vessels (perivasculitis; **c** and **h**), bronchus (peribronchitis; **d** and **i**), bronchioles (peribronchiolitis; **e** and **j**), alveolar lumen (alveolitis; **f** and **k**) and lung interstitium (interstitial pneumonitis; **g** and **l**) in lung tissues were scored ranging from 0 to 4 points, according to the number of layers of inflammatory cells. Error bars represent mean values with SD. **m**–**p** To determine EC_{50} of h5B11 in RSV-challenged cotton rats, the correlations of serum antibody concentrations with viral titers in lungs and noses were analyzed and in vivo EC_{50} values were calculated using a nonlinear regression analysis. Four to five cotton rats were used per dose group ($n = 4$–5). Points represent observed data. The solid lines indicate nonlinear regression fit of the inhibitory sigmoidal dose-response model with variable slope for RSV A lung (**m**), RSV A nose (**n**), RSV B lung (**o**), and RSV B nose (**p**). The sigmoidal dashed lines represent 95% confidence bands. The horizontal dotted lines represent the average pfu/g tissue for the naïve challenged controls. Kruskal-Wallis test was used for statistical differences between groups and corrected for multiple comparisons using Dunn's method. Source data are provided as a Source Data file.

(Fig. 1c, d), achieving a balanced antiviral efficacy against infections by RSV A and B strains (Figs. 1e–i, 5b, c and 7a, b).

Nirsevimab targets site Ø, which located on the apex region of the pre-F protein, identified as an immunodominant site prone to frequent high-risk mutations[28]. Structural-based sequence analysis has revealed the lower conservation of the epitope residues of nirsevimab (Fig. 3d). Recently epidemiological studies have spotlighted the emergence of amino acid variations at site Ø on RSV F[46,47], heightening concerns over potential antibody-resistant mutations. In the phase IIb trial of nirsevimab, two antibody-resistant clinical isolates featuring amino acid substitutions at site Ø were documented[29]. Additionally, there also exists a risk of variations in other neutralization epitopes on the pre-F. For instance, REGN2222 (suptavumab) encountered failure in a phase III trial due to the substitutions L172Q/S173L at site V across nearly all circulating RSV B strains[48]. Despite this, the 5B11-binding epitope, located within site V, relies on key amino acids other than L172/S173, and variation at residue 169 (S/N) between the two subtypes does not affect 5B11's neutralization efficacy, indicating the higher conservation of its binding site. Furthermore, no 5B11-resistant escape mutants were identified through 12 rounds of rigorous selection, suggesting that mutations within the 5B11 epitope are unlikely even under substantial immune pressure. In contrast, two variants resistant to nirsevimab (K68E/N208Y and N208S) emerged. It is noteworthy that the K68E and N208S substitutions, although rare in both RSV A and B strains, diminish nirsevimab's neutralization, as revealed by the considerably decreased susceptibility in naturally occurring variants (< 1%)[29,49,50]. Notably, the N208Y substitution in RSV A, induced under nirsevimab's selective pressure but absent in natural strains, significantly contributes to neutralization escape, particularly when combined with N67I mutation, as previously reported[50]. In this study, the detection of concurrent emergence of N208Y and K68E in nirsevimab-resistant mutants highlighted the significant impact of alterations at positions 68 and 208 on nirsevimab's binding efficacy and viral neutralization susceptibility. This highlights the superior conserved and immunologically tolerant nature that the binding site of 5B11 is more than that of nirsevimab. These findings advocate for the development of prophylactic RSV neutralizing antibodies that target highly conserved sites to diminish the emergence of resistant variants, presenting them as more favorable candidates.

In this work, we present a potent and broad-spectrum RSV neutralizing antibody 5B11, isolated from murine hybridoma cells and subsequently humanized. This antibody demonstrates robust neutralization against both laboratory strains and a variety of clinical isolates of RSV. Significantly, our study simultaneously offers cryo-EM structural insights of 5B11 in complex with the pre-F proteins of both RSV-A and RSV-B, shedding light on the underlying broad neutralization mechanism. These structures reveal that 5B11 targets site V on the pre-fusion RSV F protein, and detailed analysis of the interaction interface shows that the binding site is highly conserved across strains, with approximately 100% conservation of the contact residues. This high level of conservation of the 5B11-binding site is a more conserved region than other sites such as site Ø. Moreover, under the current screening conditions, the absence of 5B11-resistant mutants underscores the higher immunological tolerance for the 5B11 epitope compared to that targeted by nirsevimab, the potential for 5B11 to have a lower incidence of resistance development and further substantiates its promising application prospects.

The in vivo prophylactic and therapeutic studies revealed that 5B11 and its variants (h5B11 and h5B11-YTE) demonstrated potent and broad antiviral effectiveness against both RSV-A and -B subgroups. In the prophylactic setting, only 1.5 mg/mL of 5B11 could significantly inhibit viral replication in the lower respiratory tract, reduce the viral loads of the upper respiratory tract, and alleviate pulmonary inflammation—effects that were comparable to a much higher dose of 1129. In the treatment setting, 5B11 at a high dosage (15 mg/kg) therapeutically accelerated viral clearance in the lungs and the nasal turbinates, remarkably alleviated pulmonary inflammation, especially alveolitis and interstitial pneumonitis. These findings suggest the potential of 5B11 as an immunotherapeutic agent against RSV. However, the usage of RSV-neutralizing antibodies or nanobodies for antiviral therapy remains controversial. These antibodies appear to only exhibit antiviral effects but not anti-inflammatory effects. William J. Rodriguez and colleagues reported RSV immunoglobulin (RSVIG) treatment of RSV lower respiratory tract infection among previously healthy children. Although the RSVIG treatment was deemed safe and generally well-tolerated, it failed to reduce hospitalization and ICU stays[51]. Likewise, the treatment administration of conventional RSV-neutralizing antibodies (palivizumab and motavizumab) or novel trivalent nanobody (ALX-0171) did not offer clinical benefits to RSV-infected patients[52–54]. The combination of antiviral mAbs and anti-inflammatory agents appears promising in the near future[55].

Additionally, h5B11 and h5B11-YTE also demonstrated efficacious preventive effects against infections by A2 and B18537 strains in the animals. Conversely, nirsevimab was not as effective in reducing viral loads of B18537 in cotton rats. Although h5B11-YTE exhibited an eightfold increase in affinity for hFcRn at pH 6.0, compared to h5B11-WT and demonstrated a prolonged serum half-life in the hFcRn transgenic mice, comparable to that of nirsevimab, its in vivo half-life needs to be further evaluated in additional animal models, such as nonhuman primates (NHPs).

In summary, our study introduces 5B11 as a promising broad-spectrum nAb against RSV, making it a valuable antibody candidate for infant and children immunoprophylaxis, due to its broad-spectrum efficacy and lower risk of eliciting resistant mutations.

Methods

Study design

The primary objective of this study was to evaluate the potential for developing an RSV-neutralizing antibody candidate for passive prophylaxis against RSV in infants and children. RSV neutralization assays were used to validate the neutralizing abilities of the antibody candidate 5B11 and its humanized version, h5B11, against RSV laboratory

strains as well as a diverse panel of RSV A and B clinical isolates. The binding activities of these antibodies were quantified using ELISA and SPR analyses. In addition, to determine the 5B11-binding epitope and explore the structural basis of 5B11 neutralization, we solved the cryo-EM structure of 5B11 Fab bound to the RSV pre-F proteins derived from RSV strains A2 and B18537. The in vitro selection of 5B11-resistant mutants was performed to identify critical residues resulting in neutralization escape from 5B11. In vivo research experiments were designed to assess the antiviral efficacy of 5B11 and its variants (h5B11 and h5B11-YTE) against RSV infections in cotton rat or mouse model ($n = 4$ to 6 animals per group). Moreover, the PK characteristics of h5B11-YTE was evaluated in human FcRn transgenic mice ($n = 4$ mice per group, two females and two males). All work with animals was approved by the Xiamen University Laboratory Animal Management Ethics Committee. All manipulations were strictly conducted in accordance with animal ethics guidelines.

Animals

Female cotton rats of 6–8 weeks old were purchased from Envigo, USA. Female Balb/C mice of 10 weeks old were purchased from Shanghai SLAC Laboratory Animal Co., Ltd, China. Human FcRn transgenic mice C57BL/6JGpt-Fcgrt$^{em1Cin(hFCGRT)}$/Gpt were purchased from GemPharmatech Co., Ltd, China. All animals were housed in specific pathogen-free (SPF) animal facilities on a 12-hour light/dark cycle under ambient conditions with free access to food and water. The relative humidity was kept at 45 to 65%. Animal rooms and cages were kept at a temperature range of 20 to 24 °C. Viral infection was conducted in a BSL-2 facility in accordance with the guidelines for the care and use of laboratory animals.

Cells and viruses

HEp-2 cells (ATCC, CCL-23™) were cultured in Eagle's minimal essential medium (Gibco, Cat. #42360099) with 10% fetal bovine serum (Gibco, Cat. #10099141), glutamine (Invitrogen, Cat. #25030-081), penicillin and streptomycin (Invitrogen, Cat. #15140-122). Viral stocks of RSV laboratory strains (RSV A2, RSV Long, RSV B9320 and RSV B18537) and a panel of 25 RSV A and B clinical isolates were prepared and maintained as previously described[56]. The titers of the viral stocks were determined by RSV plaque assay.

Isolation of antibody 5B11

The immunization strategy for animals and the 5B11 isolation methodology were conducted as what was reported previously[18,40]. In brief, six-week-old female Balb/C mice, purchased from Shanghai SLAC Laboratory Animal Co., Ltd, China, received a primary immunization of 100 μg of DNA-F (a plasmid encoding the wild-type RSV A2 F protein) per mouse via rapid tail vein injections under high pressure. These animals were subsequently given a booster of 10^6 infection units of rAd-F (recombinant adenovirus encoding the RSV A2 F protein) per mouse through tail vein injections at four and six weeks after the primary vaccination, respectively. Two weeks after the second booster, spleen immunization was performed on mice with the highest serum neutralization titers by direct injection of 10^6 pfu of RSV A2 per mouse into the spleen. Spleens were harvested three days post spleen immunization. Spleen cells were then fused with Sp2/0 myeloma cells (ATCC, CRL-1581™) following standard protocols as described previously[57]. Positive hybridomas were identified using an RSV neutralization assay and then subcloned three times using limiting dilution method. Finally, the stable monoclonal hybridomas were injected into the peritoneal cavity of mice to generate ascites fluid.

Production and purification of RSV F mAbs and Fabs

The heavy and light chain variable region sequences of murine 5B11, h5B11, 1129 and biosimilars of palivizumab and nirsevimab were synthesized and cloned into the pVRC8400 expression vector (a gift from the National Institutes of Health) with either mouse or human constant domains (mouse IgG2a or human IgG1 for the heavy chain; kappa for the light chain). The heavy chain of h5B11-YTE was constructed by introducing the YTE modification into the heavy chain constant region of h5B11. The heavy and light chain plasmids of mAbs were co-transfected transiently into ExpiCHO-S™ cells (Thermo Fisher Scientific, Cat. #A29127) grown in suspension. After 14 days of culture, the cell supernatants were harvested, centrifuged, filtered and passed through a protein A agarose column (GenScript, Cat. #L00210). After washing and elution, the eluate was dialyzed against 1× phosphate buffer saline (PBS) at pH 7.2. Fab fragments were generated by digesting IgGs with papain (Sigma-Aldrich, Cat. #P4762) and removing IgG and Fc contaminants using a protein A agarose column.

Expression and purification of the RSV F proteins

The expression and purification of the pre-fusion and post-fusion RSV F proteins were performed as previously mentioned[18]. In brief, RSV fusion proteins were expressed by transient transfection of plasmids encoding the pre-F (DS-Cav1 for RSV A2; DS-Cav1 and sc9-10 DS-Cav1 for B18537) or post-F protein into Expi293F™ cells (Thermo Fisher Scientific, Cat. #A14528) in suspension culture. 7 days after transfection, cell culture supernatants were collected, centrifuged to remove cell debris and sterilized through filtration. The RSV F proteins were purified using a Ni sepharose fast-flow 6 resin (GE Healthcare, USA), followed by further concentration and purification on HiLoad 16/600 Superdex 200 pg size exclusion column (GE Healthcare, USA) according to the manufacturer's instructions. The purified trimeric F proteins were then concentrated, aliquoted and stored at −80 °C.

RSV plaque reduction neutralization assay

RSV plaque neutralization experiments were used to evaluate the neutralization titers of RSV mAbs against RSV laboratory strains and clinical isolates. In brief, antibodies were added to cell culture medium at 10 μg per well and was serially diluted by 5-fold to 10 gradients. An equal volume of virus was added to serial dilutions of antibodies in 96-well microplates and incubated at 37°C for 1 h. Then 100 μL per well of the antibody-virus mixture was added to 12-well microplates seeded with HEp-2 cells and the plates were incubated at room temperature for 1 h. The cells were next overlaid with 1.5 mL of EMEM medium supplemented with 1% methylcellulose and 2% FBS. After incubation at 37 °C with 5% CO_2 for 3 days, the cells were fixed with 10% neutral-buffered formalin and staining with hematoxylin and eosin stains (H&E). Plaques were counted and data were used for the non-linear fitting in GraphPad Prism 8 (GraphPad Software Inc., San Diego CA).

ELISA

The binding abilities of RSV F mAbs to the RSV F proteins was determined using ELISA as depicted previously[38]. Briefly, 96-well microtiter plates were coated with 100 ng per well of either the prefusion or postfusion RSV F protein and incubated for 2 h at 37 °C. Subsequently, 100 μL of 10-fold serially diluted antibody was added to each well and the plates were incubated for an additional hour at 37 °C. The wells were then washed five times. Next, 100 μL of horseradish peroxidase (HRP)-conjugated goat anti-mouse (Abcam, Cat. #ab97265) or anti-human IgG Fc antibody (Abcam, Cat. #ab97225) at 1:5000 was added to each well for 1 h at 37 °C. After 5 rinses, 100 μL per well of 3,3,5,5-tetramethylbenzidine (TMB) substrate solution (Wantai BioPharm, China) was added, followed by incubation at 37 °C for 10 min. The reaction was stopped by adding 50 μL of 2 M H_2SO_4 to each well, and the optical density (OD) value was determined at 450 nm with a reference wavelength of 630 nm. The half-effective concentration (EC_{50}) was calculated using sigmoid trend fitting in GraphPad Prism software (GraphPad Software, CA, USA).

For the determination of serum antibody concentration, a sandwich ELISA assay was conducted. In brief, 96-well microtiter plates

were coated with 200 ng/well of goat anti-human IgG (Fab specific) antibody (Sigma-Aldrich, Cat. #I5260) and then incubated at 37 °C for 4 h. IgG from human serum (Sigma-Aldrich, Cat. #I4506), used as the standard reference, was 2-fold serially diluted for 12 gradients, starting at a concentration of 5 μg/mL. The serially diluted serum and standard samples were added at 100 μL/well into the microplates, respectively and incubated at 37 °C for 1 h. After washing five times, 100 μL of HRP-conjugated goat anti-human IgG Fc antibody (Abcam, dilution 1:5000) was added to each well and incubated for an additional hour at 37 °C. After 5 rinses again, 100 μL per well of TMB substrate solution (Wantai BioPharm, China) was added to the plates, followed by a 10-minute incubation at 37 °C. Next, 50 μL per well of 2 M H_2SO_4 was added to stop the reaction. The OD values were measured at 450 nm with a reference wavelength of 630 nm. A standard curve was plotted based on the standard product concentrations and the corresponding OD values, facilitating the calculation of sample concentrations according to the generated standard curve.

RSV attachment inhibition assay

The efficacy of antibodies to inhibit RSV attachment to cells was determined as described previously[18,23]. Briefly, HEp-2 cells were prepared into single cell suspensions, washed twice with cold PBS, seeded into 96-well U-bottom plates, and chilled for 1 h at 4 °C prior to the experiment. Serially-diluted antibodies were mixed with RSV A2 strain and incubated for one hour at 37 °C. Heparin (Sangon, China, Cat. # 9041-08-1) served as the control inhibitor. Subsequently, the medium was discarded from the chilled cells following centrifugation (300 × g), and the mixture of virus and antibody or virus and control reagents was transferred to the chilled cells, followed by an incubation of one hour at 4 °C. Post-incubation, Hep-2 cells were washed with cold PBS to remove unbound viruses and fixed with 0.5% paraformaldehyde. Virus attached to the cell surface was labeled using Dylight 488-conjugated antibody 1129. After three washes with cold PBS, cells with virus attachment were analyzed using LSRFortessa™ X-20 (BD Biosciences).

RSV fusion inhibition assay

The efficacy of antibodies to inhibit RSV-induced virus-to-cell fusion was assessed as reported previously[18,23]. In brief, Hep-2 cells were pre-seeded in 96-well cell-culture plates and cultured at 37 °C for 24 h, followed by chilling for one hour at 4 °C before the experiment. RSV A2-mKate (RSV strain A2 carrying the monomeric Katushka fluorescent protein) was added to pre-chilled cells at 4 °C. Subsequently, the cells were washed with cold PBS to remove unbound viruses. Serial dilutions of antibodies were then added to the chilled cells and incubated for 1 h at 4 °C. After incubation at 37 °C for 24 h, the fluorescence intensity in each well was quantified by using a fluorescence plate reader (SpectraMax Paradigm, Molecular Devices, Sunnyvale, CA, USA).

Affinity determination using SPR

The binding affinities of 5B11-Fab and niservimab-Fab towards RSV strain A2 or B18537 DS-Cav1 were determined by SPR using a Biacore 8 K instrument (Cytiva), which were performed in 1×PBS-P+ buffer (Cytiva) with 2% DMSO. In brief, the flow duration was 200 s for the association stage and 10 min for the dissociation stage. The NTA sensor chip surface (Cytiva) was activated with 0.5 mM NiSO4 solution and 0.5 μg/mL of the trimeric DS-Cav1 with His-tag was captured on the sensor chip at a flow rate of 10 μL/min for 180 s. Then, serial dilutions of the purified Fabs as the analyte were injected at 30 μL/min for association of 180 s and dissociation of 600 s. After each cycle, the sensor was regenerated with 350 mM EDTA. The response data were fit to a 1:1 binding model using Biacore 8 K analysis software (Cytiva). To measure binding kinetics of mAbs for hFcRn (MedChemExpress, Cat. #HY-P70601) at pH 6.0, antibodies were immobilized on CM5 chip surface via an amine coupling. Phosphate buffer at pH 6.0 was used as the running buffer, while HBS-P+ buffer at pH 7.4 was used as the regeneration buffer. Serial dilutions of hFcRn were injected over immobilized mAbs at pH 6.0 with a flow rate of 50 μl/min. K_D values for mAb binding were determined at pH 6.0 by fitting data to a 1:1 binding isotherm equation using Biacore evaluation software (Cytiva).

Cryo-EM sample preparation and data collection

Purified A2 DS-Cav1 was incubated with 5B11 Fab overnight at a molar ratio of 1.2 at 4 °C. 5B11:A2 DS-Cav1 complex was then purified to remove any excess Fab on HiLoad 16/600 Superdex 200 pg size exclusion column (GE Healthcare, USA) in 10 mM Tris pH 8.0 with 50 mM NaCl. The purified complex at a concentration of ~2.0 mg/mL were incubated in 0.01% (v/v) Digitonin and immediately frozen on a glow-discharged (80 s at 20 mA) holey carbon Quantifoil grids (R1.2/1.3, 300 mesh, Quantifoil Micro Tools) using a Vitrobot Mark IV (Thermo Fisher Scientific) at 100% humidity and 4 °C. Similarly, purified B18537 sc9-10 DS-Cav1 was incubated with 5B11 Fab at a molar ratio of 1.2 for 30 min at 37 °C. The resulting complex was then mixed with 0.25 mM DDM and loaded onto glow-discharged (80 s at 20 mA) holey Au Quantifoil grids (R1.2/1.3, 300 mesh, Quantifoil Micro Tools) using a Vitrobot Mark IV (ThermoFisher Scientific) at 100% humidity and 4 °C. Both datasets were acquired on a Tecnai F30 transmission electron microscope (ThermoFisher Scientific) operating at 300 kV and equipped with a Gatan K3 direct electron detector. Images were collected using the SerialEM 3.8.5 software at a nominal magnification of 39,000× at super-resolution mode with a pixel size of 0.389 Å and a total electron dose of 60 e^{-} $Å^{-2}$.

Image processing and 3D reconstruction

All dose-fractioned images were motion-corrected and dose-weighted by MotionCor2[58] and their Contrast transfer function (CTF) parameters were estimated using the Gctf[59]. Low-quality images were discarded before reconstruction. The following reconstruction procedures (summarized in Figs. S4, S5) were performed by using cryoSPARC v3[60]. In short, particles were automatically picked by using the "Blob picker" or "Template picker" and selected through several rounds of reference-free 2D classifications. The selected good particles were then subjected to ab-initio reconstruction, heterogeneous refinement and non-uniform refinement. Due to the flexibility in the antibody interface regions, localized refinements of regions of A2 DS-Cav1:5B11 and B18537 sc9-10 DS-Cav1:h5B11, were performed by specific local masks to improve the quality of cryo-EM density maps. The maps of localized refinement were used for further model building. The final resolution was determined by gold-standard Fourier shell correlation (FSC) between the two independently refined half maps, with a cutoff of 0.143[61]. Local map resolution was estimated with ResMap[62].

Model building, refinement and 3D visualization

The initial models of mAbs were generated from homology modeling by Accelrys Discovery Studio software (available at https://www.3dsbiovia.com). For the A2 DS-Cav1:5B11 complex, the structure of DS-Cav1 (PDB: 7MPG) served as the initial model for A2 DS-Cav1. Similarly, the structure of DS-Cav1 (PDB: 6Q0S) was employed as the initial model for the B18537 sc9-10 DS-Cav1:h5B11 complex. The initial templates were fitted into the corresponding cryo-EM maps using Chimera[63], followed by manual corrections and adjustments using real-space refinement in Coot[64]. The resulting models were further refined with phenix.real_space_refine in PHENIX[65]. Iterative cycles of manual model adjustment in COOT and real-space refinement in Phenix were performed. The final atomic models were validated using Molprobity[66]. The statistics of cryo-EM data processing and refinement are summarized in Table S1. The buried surface areas and interactions were analyzed using PISA server (https://www.ebi.ac.uk/pdbe/pisa/) and the CCP4 program[67]. Structural representations were generated

using Chimera or ChimeraX[68]. The electron density map and corresponding models of α-helices in the RSV A2 DS-Cav1:5B11 and RSV B18537 sc9-10 DS-Cav1:h5B11 complexes are depicted in Fig. S7, where the density map of NAG ligand binding to DS-Cav1 in the RSV A2 DS-Cav1:5B11 complex is also shown.

In vitro selection of antibody-resistant mutants

5B11 or nirsevimab at an initial concentration of 50 ng/mL was mixed with a stock of RSVA2-mKate and incubated at 37 °C for 1 h. The antibody-virus mixture was then transferred into 12-well plates seeded with HEp-2 cells, followed by 3 days incubation at 37 °C. Cytopathic effects were observed daily using fluorescence microscopy. 3 days later, the contents of each well were harvested for ultrasonication, followed by centrifugation at 4 °C and 600 × *g* for 20 min. The supernatant was used for next round of selection as described above. The selection process of each antibody concentration was repeated two times. The resistant mutants were cloned 3 times by plaque assay. Finally, the viral F genes were amplified using reverse transcription-polymerase chain reaction (RT-PCR) and subsequently sequenced via the Sanger method.

RSV prophylaxis and treatment assays

In the prophylactic setting, female cotton rats of 6–8 weeks old were administered intramuscularly (IM) with desired doses of RSV F mAbs based on the body weight of each animal ($n = 4$ to 6 animals per group). 24 h later, the cotton rats were inoculated intranasally with RSV strain A2 or B18537 under isoflurane anesthesia. For in-vivo EC_{50} evaluation, h5B11, with initial concentration of 3 mg/kg, was serially diluted 3-fold to 0.033 mg/kg. A total of 5 antibody dose groups were tested (3, 1, 0.33, 0.11, 0.033 mg/kg). Approximately 24 h after antibody administration, blood samples were collected for evaluating serum antibody level with ELISA. Subsequently, each animal was immediately challenged intranasally as described above. 5 days after RSV inoculation, the cotton rats were sacrificed with CO_2 inhalation. Their right lung lobes and nasal turbinates were harvested, flash frozen and immediately stored at −80 °C until thawed for viral titration. The viral titers in lungs or noses were evaluated in a plaque assay. The limit of detection of virus was 200 PFU/g for the bisected lungs and 100 PFU/g for nose samples. Their left lung lobes were isolated and fixed using 10% formalin for hematoxylin and eosin stains (H&E) histological section.

In the therapeutic setting, female Balb/C mice of 10 weeks old were inoculated intranasally with RSV strain A2 under isoflurane anesthesia ($n = 5$ mice per group). One day after RSV challenge, animals were administrated intramuscularly with 5 mg/kg or 15 mg/kg of antibodies. Lung and nasal tissues from each group of mice were harvested at day 5 post-infection. The quantification of viral titers in lungs and nasal turbinates and histology scores of lungs were performed according to the prophylaxis studies.

Histopathological scores of lungs

At day 5 post infection, lung tissues of RSV-infected animals were harvested. Left lungs were immediately fixed in 10% neutral-buffered formalin solution, subsequently paraffin-embedded as well as H&E stains. All lung sections were randomly numbered and the histopathologist was blinded to the information about lung tissue and the entire set of slides. The pathology scoring system provided 0–4 points for each lung section, based on the level of inflammatory cell infiltration around bronchus (peribronchitis), bronchioles (peribronchiolitis), small blood vessels (perivasculitis), alveolar lumen (alveolitis) and lung interstitium (interstitial pneumonitis) in the lung tissues. Each sagittal section was scored as shown in Table S2.

Pharmacokinetics studies

PK studies for the long-acting h5B11-YTE were performed in human FcRn transgenic mice. Four mice (2 females and 2 males) were randomly assigned to each group. Mice were IM injected with antibodies of 10 mg/kg. Blood samples were collected at 2 h, 24 h, 72 h, 120 h, 168 h, 240 h and 360 h post-injection. Serum antibody concentrations were tested using a quantified ELISA assay. A line graph plotting the mean serum concentration vs hours post dose was generated by GraphPad Prism 8 software. Half-life is calculated using the formula:

$$t\frac{1}{2} = \frac{\log(0.5)}{\log\left(\frac{Ae}{Ao}\right)} \times t$$

where $t_{1/2}$ is the serum half-life of the antibody, Ae is the amount of antibody remaining, and A0 is the original amount of antibody at day 0 and t is the elapsed time[69].

Statistical analysis

Lines present in the graphs represent the mean as indicated. One-way ANOVA was applied to analyze the differences of lung and nose titers between groups and corrected for multiple comparisons using Tukey's method. Kruskal-Wallis test was used to analyze the differences of histopathological scores of lungs between groups and corrected for multiple comparisons using Dunn's method. Two-tailed *P* values of <0.05 were statistically significant. All statistical analyses were performed in the GraphPad Prism 8 software.

Reporting summary

Further information on research design is available in the Nature Portfolio Reporting Summary linked to this article.

Data availability

Source data are provided as a Source Data file. Source data are provided with this paper. The cryo-EM structures in this study have been deposited in the Protein Data Bank under accession codes 8WZ3, 8WZ4, 8WZ5 and 8WZE. Other structures for analysis, including 7MPG, 5W23, 5UDC, 7MMN, 5TPN, 3IXT, 5U68, 6OUS, 6W52, 6OE4 and 6Q0S were obtained from the PDB. The fusion protein sequences of RSV clinical isolates in this study are available as supplementary data and have been submitted to NCBI GenBank (GenBank accession numbers PQ538809-PQ538833). Additionally, the F protein sequences from two nirsevimab-resistant mutants have been deposited in GenBank (GenBank accession numbers PQ535507 and PQ535508). Source data are provided with this paper.

References

1. Benet, T. et al. Microorganisms associated with pneumonia in children <5 years of age in developing and emerging countries: the gabriel pneumonia multicenter, prospective, case-control study. *Clin. Infect. Dis.* **65**, 604–612 (2017).
2. Shi, T. et al. Global disease burden estimates of respiratory syncytial virus-associated acute respiratory infection in older adults in 2015: a systematic review and meta-analysis. *J. Infect. Dis.* **222**, S577–S583 (2020).
3. Tabor, D. E., et al. Global molecular epidemiology of respiratory syncytial virus from the 2017-2018 inform-rsv study. *J. Clin. Microbiol.* **59**, e01828-20 (2020).
4. O'Brien, K. L. et al. Causes of severe pneumonia requiring hospital admission in children without HIV infection from Africa and Asia: the PERCH multi-country case-control study. *Lancet* **394**, 757–779 (2019).
5. Li, Y. et al. Global, regional, and national disease burden estimates of acute lower respiratory infections due to respiratory syncytial virus in children younger than 5 years in 2019: a systematic analysis. *Lancet* **399**, 2047–2064 (2022).
6. Kingwell, K. RSV vaccines score landmark FDA approvals. *Nat. Rev. Drug Discov.* **22**, 523–525 (2023).

7. Mullard, A. FDA approves mRNA-based RSV vaccine. *Nat. Rev. Drug Discov.* **23**, 487–487 (2024).
8. Drysdale, S. B., et al. Priorities for developing respiratory syncytial virus vaccines in different target populations. *Sci. Transl. Med.* **12**, 535 (2020).
9. Chu, H. Y. et al. Respiratory syncytial virus transplacental antibody transfer and kinetics in mother-infant pairs in Bangladesh. *J. Infect. Dis.* **210**, 1582–1589 (2014).
10. Brandenburg, A. H. et al. Respiratory syncytial virus specific serum antibodies in infants under six months of age: limited serological response upon infection. *J. Med Virol.* **52**, 97–104 (1997).
11. Munoz, F. M., Piedra, P. A. & Glezen, W. P. Safety and immunogenicity of respiratory syncytial virus purified fusion protein-2 vaccine in pregnant women. *Vaccine* **21**, 3465–3467 (2003).
12. Ochola, R. et al. The level and duration of RSV-specific maternal IgG in infants in Kilifi Kenya. *PLoS One* **4**, e8088 (2009).
13. Madhi, S. A. et al. Respiratory Syncytial Virus Vaccination during Pregnancy and Effects in Infants. *N. Engl. J. Med* **383**, 426–439 (2020).
14. Ruckwardt, T. J. The road to approved vaccines for respiratory syncytial virus. *Npj Vaccines* **8**, 138 (2023).
15. Boytchev, H. FDA advisers back Pfizer's maternal RSV vaccine after voicing safety concerns. *BMJ* **381**, 1187 (2023).
16. McLellan, J. S. Neutralizing epitopes on the respiratory syncytial virus fusion glycoprotein. *Curr. Opin. Virol.* **11**, 70–75 (2015).
17. Rossey, I., McLellan, J. S., Saelens, X. & Schepens, B. Clinical potential of prefusion rsv f-specific antibodies. *Trends Microbiol* **26**, 209–219 (2018).
18. McLellan, J. S. et al. Structure of RSV fusion glycoprotein trimer bound to a prefusion-specific neutralizing antibody. *Science* **340**, 1113–1117 (2013).
19. Mousa, J. J., Kose, N., Matta, P., Gilchuk, P. & Crowe, J. E. Jr. A novel pre-fusion conformation-specific neutralizing epitope on the respiratory syncytial virus fusion protein. *Nat. Microbiol* **2**, 16271 (2017).
20. Anderson, L. J., Bingham, P. & Hierholzer, J. C. Neutralization of respiratory syncytial virus by individual and mixtures of F and G protein monoclonal antibodies. *J. Virol.* **62**, 4232–4238 (1988).
21. Null, D. et al. Palivizumab, a humanized respiratory syncytial virus monoclonal antibody, reduces hospitalization from respiratory syncytial virus infection in high-risk infants. *Pediatrics* **102**, 531–537 (1998).
22. Wen, X. et al. Structural basis for antibody cross-neutralization of respiratory syncytial virus and human metapneumovirus. *Nat. Microbiol* **2**, 16272 (2017).
23. McLellan, J. S. et al. Structure of a major antigenic site on the respiratory syncytial virus fusion glycoprotein in complex with neutralizing antibody 101F. *J. Virol.* **84**, 12236–12244 (2010).
24. Palivizumab, a humanized respiratory syncytial virus monoclonal antibody, reduces hospitalization from respiratory syncytial virus infection in high-risk infants. The IMpact-RSV Study Group. *Pediatrics* **102**, 531–537 (1998).
25. Brady, M. T. et al. Updated guidance for palivizumab prophylaxis among infants and young children at increased risk of hospitalization for respiratory syncytial virus infection. *Pediatrics* **134**, E620–E638 (2014).
26. Zhu, Q. et al. A highly potent extended half-life antibody as a potential RSV vaccine surrogate for all infants. *Sci. Transl. Med.* **9**, eaaj1928 (2017).
27. Tutwiler, K. & Toussaint, J. F. Deliver Best-in-Class RSV franchise. https://www.sanofi.com/assets/dotcom/content-app/events/investor-presentation/2023/vaccines-investor-event/presentation-vaccines-event-2023.pdf (2023).
28. Tang, A. et al. A potent broadly neutralizing human RSV antibody targets conserved site IV of the fusion glycoprotein. *Nat. Commun.* **10**, 4153 (2019).
29. Griffin, M. P. et al. Single-dose nirsevimab for prevention of rsv in preterm infants. *N. Engl. J. Med* **383**, 415–425 (2020).
30. Caban, M. et al. Cross-protective antibodies against common endemic respiratory viruses. *Nat. Commun.* **14**, 798 (2023).
31. Gilman, M. S. A. et al. Transient opening of trimeric prefusion RSV F proteins. *Nat. Commun.* **10**, 2105 (2019).
32. Mousa, J. J. et al. Human antibody recognition of antigenic site IV on Pneumovirus fusion proteins. *PLoS Pathog.* **14**, e1006837 (2018).
33. Harshbarger, W. et al. Convergent structural features of respiratory syncytial virus neutralizing antibodies and plasticity of the site V epitope on prefusion F. *PLoS Pathog.* **16**, e1008943 (2020).
34. Wen, X. et al. Potent cross-neutralization of respiratory syncytial virus and human metapneumovirus through a structurally conserved antibody recognition mode. *Cell Host Microbe* **31**, 1288–1300.e1286 (2023).
35. Mejias, A., et al. Motavizumab, a neutralizing anti-respiratory syncytial virus (Rsv) monoclonal antibody significantly modifies the local and systemic cytokine responses induced by Rsv in the mouse model. *Virol. J.* **4**, 109 (2007).
36. O'Brien, K. L. et al. Efficacy of motavizumab for the prevention of respiratory syncytial virus disease in healthy Native American infants: a phase 3 randomised double-blind placebo-controlled trial. *Lancet Infect. Dis.* **15**, 1398–1408 (2015).
37. Feltes, T. F. et al. A randomized controlled trial of motavizumab versus palivizumab for the prophylaxis of serious respiratory syncytial virus disease in children with hemodynamically significant congenital heart disease. *Pediatr. Res* **70**, 186–191 (2011).
38. Zhao, M. et al. Discovery of a prefusion rsv f-specific monoclonal antibody that provides greater in vivo protection than the murine precursor of palivizumab. *J. Virol.* **91**, e00176–00117 (2017).
39. Tian, D. et al. Structural basis of respiratory syncytial virus subtype-dependent neutralization by an antibody targeting the fusion glycoprotein. *Nat. Commun.* **8**, 1877 (2017).
40. McLellan, J. S. et al. Structure-based design of a fusion glycoprotein vaccine for respiratory syncytial virus. *Science* **342**, 592–598 (2013).
41. Joyce, M. G. et al. Iterative structure-based improvement of a fusion-glycoprotein vaccine against RSV. *Nat. Struct. Mol. Biol.* **23**, 811–820 (2016).
42. Gilman, M. S. et al. Characterization of a prefusion-specific antibody that recognizes a quaternary, cleavage-dependent epitope on the RSV fusion glycoprotein. *Plos Pathog.* **11**, e1005035 (2015).
43. McLellan, J. S. et al. Structural basis of respiratory syncytial virus neutralization by motavizumab. *Nat. Struct. Mol. Biol.* **17**, 248–250 (2010).
44. Robbie, G. J. et al. A novel investigational Fc-modified humanized monoclonal antibody, motavizumab-YTE, has an extended half-life in healthy adults. *Antimicrob. Agents Chemother.* **57**, 6147–6153 (2013).
45. Loo, Y. M. The SARS-CoV-2 monoclonal antibody combination, AZD7442, is protective in nonhuman primates and has an extended half-life in humans (vol 14, eabg8900, 2022). *Sci. Transl. Med.* **14** (2022).
46. Sun, Y. P., et al. Molecular Evolution of Attachment Glycoprotein (G) and Fusion Protein (F) Genes of Respiratory Syncytial Virus ON1 and BA9 Strains in Xiamen, China. *Microbiol. Spectr.* e0208321 (2022).
47. Bin, L. et al. Emergence of new antigenic epitopes in the glycoproteins of human respiratory syncytial virus collected from a US surveillance study, 2015-17. *Sci. Rep.* **9**, 3898 (2019).
48. Simoes, E. A. F. et al. Suptavumab for the prevention of medically attended respiratory syncytial virus infection in preterm infants. *Clin. Infect. Dis.* **73**, e4400–e4408 (2021).
49. Wilkins, D. et al. Nirsevimab binding-site conservation in respiratory syncytial virus fusion glycoprotein worldwide between 1956 and

2021: an analysis of observational study sequencing data. *Lancet Infect. Dis.* **23**, 856–866 (2023).
50. Zhu, Q. et al. Prevalence and significance of substitutions in the fusion protein of respiratory syncytial virus resulting in neutralization escape from antibody MEDI8897. *J. Infect. Dis.* **218**, 572–580 (2018).
51. Rodriguez, W. J. et al. Respiratory syncytial virus immune globulin treatment of RSV lower respiratory tract infection in previously healthy children. *Pediatrics* **100**, 937–942 (1997).
52. Lagos, R. et al. Safety and antiviral activity of motavizumab, a respiratory syncytial virus (rsv)-specific humanized monoclonal antibody, when administered to rsv-infected children. *Pediatr. Infect. Dis. J.* **28**, 835–837 (2009).
53. Ramilo, O. et al. Motavizumab treatment of infants hospitalized with respiratory syncytial virus infection does not decrease viral load or severity of illness. *Pediatr. Infect. Dis. J.* **33**, 703–709 (2014).
54. Cunningham, S. et al. Nebulised ALX-0171 for respiratory syncytial virus lower respiratory tract infection in hospitalised children: a double-blind, randomised, placebo-controlled, phase 2b trial. *Lancet Respir. Med* **9**, 21–32 (2021).
55. Prince, G. A., Mathews, A., Curtis, S. J. & Porter, D. D. Treatment of respiratory syncytial virus bronchiolitis and pneumonia in a cotton rat model with systemically administered monoclonal antibody (palivizumab) and glucocorticosteroid. *J. Infect. Dis.* **182**, 1326–1330 (2000).
56. Graham, B. S., Perkins, M. D., Wright, P. F. & Karzon, D. T. Primary respiratory syncytial virus-infection in mice. *J. Med. Virol.* **26**, 153–162 (1988).
57. E. Harlow, D. P. Lane, Antibodies: A Laboratory Manual (Cold Spring Harbor Laboratory Press, Cold Spring Harbor, New York, 1988)
58. Zheng, S. Q. et al. MotionCor2: anisotropic correction of beam-induced motion for improved cryo-electron microscopy. *Nat. Methods* **14**, 331–332 (2017).
59. Zhang, K. Gctf: Real-time CTF determination and correction. *J. Struct. Biol.* **193**, 1–12 (2016).
60. Punjani, A., Rubinstein, J. L., Fleet, D. J. & Brubaker, M. A. cryoSPARC: algorithms for rapid unsupervised cryo-EM structure determination. *Nat. Methods* **14**, 290–296 (2017).
61. Scheres, S. H. & Chen, S. Prevention of overfitting in cryo-EM structure determination. *Nat. Methods* **9**, 853–854 (2012).
62. Kucukelbir, A., Sigworth, F. J. & Tagare, H. D. Quantifying the local resolution of cryo-EM density maps. *Nat. Methods* **11**, 63–65 (2014).
63. Pettersen, E. F. et al. UCSF Chimera–a visualization system for exploratory research and analysis. *J. Comput Chem.* **25**, 1605–1612 (2004).
64. Emsley, P. & Cowtan, K. Coot: model-building tools for molecular graphics. *Acta Crystallogr D. Biol. Crystallogr* **60**, 2126–2132 (2004).
65. Adams, P. D. et al. PHENIX: a comprehensive Python-based system for macromolecular structure solution. *Acta Crystallogr D. Biol. Crystallogr* **66**, 213–221 (2010).
66. Chen, V. B. et al. MolProbity: all-atom structure validation for macromolecular crystallography. *Acta Crystallogr D. Biol. Crystallogr* **66**, 12–21 (2010).
67. Potterton, L. et al. CCP4i2: the new graphical user interface to the CCP4 program suite. *Acta Crystallogr D. Struct. Biol.* **74**, 68–84 (2018).
68. Pettersen, E. F. et al. UCSF ChimeraX: Structure visualization for researchers, educators, and developers. *Protein Sci.* **30**, 70–82 (2021).
69. Roopenian, D. C., Christianson, G. J., Proetzel, G. & Sproule, T. J. Human FcRn transgenic mice for pharmacokinetic evaluation of therapeutic antibodies. *Methods Mol. Biol.* **1438**, 103–114 (2016).

Acknowledgements

This work was supported by National Natural Science Foundation of China (Grant No. 81991491 to N.S.X. and 82071783 to Z.Z.Z.); National Key Research and Development program of China (Grant No. 2022YFC2704902 to Z.Z.Z.); Fujian Natural Science Foundation (Grant No. 2022J02005 to Z.Z.Z.); CAMS Innovation Fund for Medical Sciences (Grant No. 2019RU022 to N.S.X.) and the Fundamental Research Funds for the Central Universities (Grant No. 20720220006 to N.S.X.). We thank the Women and Children's Hospital (affiliated to Xiamen University) for support on this project.

Author contributions

E.M.L., Q.B.Z., Z.Z.Z. and N.S.X. conceptualized and designed the study. Y.P.S., L.Q.L., H.S.Q., H.S., Y.C.J., L.R., Z.M.J., S.Y.L., L.C., Y.Z.W., X.L., G.S.W., Y.H., Y.H.F. Y.J.S. and X.T.C. performed experiments. Y.P.S., L.Q.L., H.S.Q., H.S., Y.C.J., L.R., Z.M.J., Q.B.Z. and Z.Z.Z. analyzed data. H.Y., S.W.L., W.X.L., L.R. and E.M.L. provided resources. Z.Z.Z. and N.S.X. acquired funding. Y.P.S., L.Q.L., H.S.Q., H.S., Y.C.J., L.R. and Z.M.J. wrote the paper. Y.P.S., L.Q.L., E.M.L., Q.B.Z., Z.Z.Z. and N.S.X. revised the manuscript.

Competing interests

The authors declare no competing interests.

Additional information

Supplementary information The online version contains supplementary material available at https://doi.org/10.1038/s41467-024-54384-x.

Correspondence and requests for materials should be addressed to Enmei Liu, Qingbing Zheng, Zizheng Zheng or Ningshao Xia.

Peer review information *Nature Communications* thanks the anonymous reviewers for their contribution to the peer review of this work. A peer review file is available.